Supporting Information

Shaped-directed dynamics of active colloids powered by induced-charge electrophoresis

Allan M. Brooks[1], Syeda Sabrina[1], and Kyle J. M. Bishop*[2]

[1]Department of Chemical Engineering, Pennsylvania State University
[2]Department of Chemical Engineering, Columbia University

*Address correspondence to kyle.bishop@columbia.edu

Contents

1 Supporting Videos **3**
- 1.1 Video S1: $\boldsymbol{D_{\infty h}}$ Rotation Class . . . 3
- 1.2 Video S2: $\boldsymbol{D_{3d}}$ Rotation Class . . . 3
- 1.3 Video S3: $\boldsymbol{C_{4h}}$ Rotation Class . . . 3
- 1.4 Video S4: $\boldsymbol{S_6}$ Rotation Class . . . 3
- 1.5 Video S5: $\boldsymbol{C_{2h}}$ Rotation Class . . . 3
- 1.6 Make your own . . . 3

2 Symmetry Group Nomenclature **4**

3 Numerical Method **5**
- 3.1 Particle Shape . . . 5
- 3.2 Electrostatics . . . 5
  - 3.2.1 Integral Equation for the Potential $\Phi(\boldsymbol{x})$ . . . 6
  - 3.2.2 Integral Equation for the Potential Gradient $\nabla\Phi(\boldsymbol{x})$ . . . 6
- 3.3 Hydrodynamics . . . 7
  - 3.3.1 Integral Equation for the Stress $\hat{\boldsymbol{f}}(\boldsymbol{x})$ . . . 7
- 3.4 Numerical Solution . . . 8
  - 3.4.1 Lebedev Quadrature . . . 8
  - 3.4.2 Electrostatics . . . 8
  - 3.4.3 Hydrodynamics . . . 9
  - 3.4.4 Error Analysis . . . 9

4 Particle Dynamics **11**
- 4.1 $D_{\infty h}$ Rotation Class . . . 11
- 4.2 D_{2h} Rotation Class . . . 14
- 4.3 D_{3d} Rotation Class . . . 16
- 4.4 C_{4h} Rotation Class . . . 18
- 4.5 S_6 Rotation Class . . . 20
- 4.6 C_{2h} Rotation Class . . . 22

5 Sensitivity on Particle Shape **25**

6 Effects of Brownian Motion **26**

7 Two-Photon Lithography **29**

1 Supporting Videos

1.1 Video S1: $D_{\infty h}$ Rotation Class

Video S1 shows the dynamics particles in the $D_{\infty h}$ rotation class, including a $D_{\infty h}$ parallel aligner, a $D_{\infty h}$ perpendicular aligner, a $C_{\infty h}$ parallel rocket, a $C_{\infty h}$ perpendicular rocket, a D_{2d} perpendicular shuttle, and a D_{3h} perpendicular glider. The shape parameters characterizing each particle are shown in the video.

1.2 Video S2: D_{3d} Rotation Class

Video S2 shows the dynamics of particles in the D_{3d} rotation class, including a D_{3d} perpendicular flipper, a D_3 perpendicular flipping glider, and a C_{3v} perpendicular flipping cruiser. The shape parameters characterizing each particle are shown in the video.

1.3 Video S3: C_{4h} Rotation Class

Video S3 shows the dynamics of particles in the C_{4h} rotation class, including a C_{4h} parallel spinner, a C_{4h} perpendicular spinner, a C_4 parallel spinning rocket, a C_4 perpendicular spinning rocket, a C_{3h} perpendicular spinning glider, and an S_4 perpendicular spinning shuttle. The shape parameters characterizing each particle are shown in the video.

1.4 Video S4: S_6 Rotation Class

Video S4 shows the dynamics of particles in the S_6 rotation class, including an S_6 precesser, an S_6 wobbler, a C_3 precessing cruiser, and a C_3 wobbling cruiser. The shape parameters characterizing each particle are shown in the video.

1.5 Video S5: C_{2h} Rotation Class

Video S5 shows the dynamics of particles in the C_2 rotation class, including a C_{2h} perpendicular spinner, a C_{2h} aligner, a C_2 perpendicular spinning shuttle, a C_s parallel spinning glider, and a C_s perpendicular spinning glider.

1.6 Make your own

A MATLAB program with which to generate your own trajectories for particles of different symmetries is available at `https://github.com/kjmbishop/shapeICEP`.

2 Symmetry Group Nomenclature

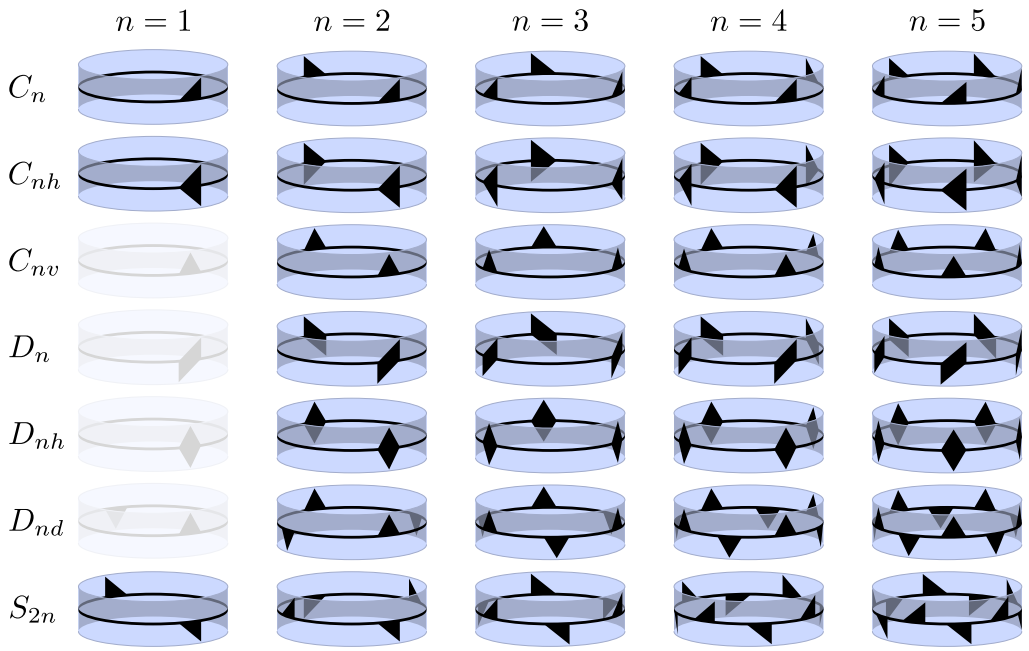

Figure S1: Patterns on a cylindrical band illustrate the seven infinite series of axial point groups of order n. Each group is labeled using its corresponding Schoenflies notation [1]. $\boldsymbol{C_n}$ has n-fold rotational symmetry and no other symmetry elements (other than the identity operation). We will refer to the n-fold rotation axis as the primary axis. $\boldsymbol{C_{nh}}$ has n-fold rotational symmetry and mirror symmetry about the plane perpendicular to the primary axis. $\boldsymbol{C_{nv}}$ has n-fold rotational symmetry and mirror symmetry about n planes parallel to the primary axis. $\boldsymbol{D_n}$ has n-fold rotational symmetry and n axes of 2-fold rotational symmetry that lie perpendicular to the primary axis. $\boldsymbol{D_{nh}}$ has the symmetries of D_n as well as mirror symmetry about the plane perpendicular to the primary axis and n planes parallel to that axis. $\boldsymbol{D_{nd}}$ has the symmetries of D_n as well as mirror symmetry about n planes parallel to the primary axis that bisect the angles separating the axes of 2-fold rotational symmetry. $\boldsymbol{S_{2n}}$ has $2n$-fold improper rotation symmetry (i.e., invariance to $2n$-fold rotation followed by inversion). In the column $n = 1$, the obscured entries appear elsewhere in the table; C_{1h} and S_2 are often denoted as C_s and C_i, respectively.

3 Numerical Method

3.1 Particle Shape

We consider particle shapes that can be expressed by the following parametric form

$$\boldsymbol{x}(\theta,\phi) = f(\theta,\phi)\left(\cos\phi\sin\theta\boldsymbol{e}_{x'} + \sin\phi\sin\theta\boldsymbol{e}_{y'} + \cos\theta\boldsymbol{e}_{z'}\right), \tag{S1}$$

where $\boldsymbol{e}_i$ is the unit vector in the i-direction, and the function $f(\theta,\phi)$ is a linear combination of spherical harmonics

$$f(\theta,\phi) = \sum_{\ell=0}^{\infty}\sum_{m=0}^{\ell}\mathrm{Re}\left(B_{\ell m}Y_\ell^m(\theta,\phi)\right), \tag{S2}$$

with coefficients $B_{\ell m}$ chosen such that $f(\theta,\phi) > 0$. In this way, the surface is fully specified by the coefficients $B_{\ell m}$. Using this parametric form, it is straightforward to compute all the surface geometric quantities needed for the subsequent analysis. To summarize, the unit vectors tangent to the surface are

$$\boldsymbol{t}^{(\theta)} = \frac{\boldsymbol{x}_\theta}{|\boldsymbol{x}_\theta|} \text{ and } \boldsymbol{t}^{(\phi)} = \frac{\boldsymbol{x}_\phi}{|\boldsymbol{x}_\phi|}, \tag{S3}$$

where the subscript θ or ϕ denotes differentiation (e.g., $\boldsymbol{x}_\theta = \partial_\theta\boldsymbol{x}(\theta,\phi)$). The outward-pointing unit vector $\boldsymbol{n}$ normal to the surface is

$$\boldsymbol{n} = \boldsymbol{t}^{(\theta)} \times \boldsymbol{t}^{(\phi)}. \tag{S4}$$

The surface integral over an arbitrary function $g(\boldsymbol{x})$ can be written as

$$\int_{S_p} g(\boldsymbol{x})dS = \int_0^\pi\int_0^{2\pi} g(\boldsymbol{x})|\boldsymbol{x}_\theta \times \boldsymbol{x}_\phi|d\phi d\theta, \tag{S5}$$

where S_p denotes the particle surface. The local mean curvature is given by

$$H = \frac{GL - 2FM + EN}{2(EG - F^2)}, \tag{S6}$$

where the coefficients of the first and second fundamental forms are given by

$$E = \boldsymbol{x}_\theta\cdot\boldsymbol{x}_\theta, \quad F = \boldsymbol{x}_\theta\cdot\boldsymbol{x}_\phi, \quad G = \boldsymbol{x}_\phi\cdot\boldsymbol{x}_\phi \tag{S7}$$

$$L = \boldsymbol{x}_{\theta\theta}\cdot\boldsymbol{n}, \quad M = \boldsymbol{x}_{\theta\phi}\cdot\boldsymbol{n}, \quad N = \boldsymbol{x}_{\phi\phi}\cdot\boldsymbol{n}. \tag{S8}$$

3.2 Electrostatics

The electric potential Φ surrounding the particle satisfies the Laplace equation

$$\nabla^2\Phi = 0. \tag{S9}$$

As there is no ionic current normal to the surface of the particle, we have

$$\boldsymbol{n}\cdot\nabla\Phi(\boldsymbol{x}) = 0 \text{ for } \boldsymbol{x}\in S_p. \tag{S10}$$

Far from the particle, the potential approaches the externally applied potential $\Phi^\infty(\boldsymbol{x})$

$$\Phi(\boldsymbol{x}) = \Phi^\infty(\boldsymbol{x}) = -\boldsymbol{E}^\infty\cdot\boldsymbol{x} \text{ for } \boldsymbol{x}\to\infty, \tag{S11}$$

where $\boldsymbol{E}^\infty$ is the constant electric field.

3.2.1 Integral Equation for the Potential $\Phi(\boldsymbol{x})$

The problem above admits the following integral solution [2] for the potential $\Phi(\boldsymbol{x})$ at point $\boldsymbol{x}$ on the particle's surface

$$\frac{1}{2}\Phi(\boldsymbol{x}) = -\int_S \mathcal{G}(\boldsymbol{y},\boldsymbol{x})[\boldsymbol{n}(\boldsymbol{y})\cdot\nabla\Phi(\boldsymbol{y})]dS(\boldsymbol{y}) + \int_S \Phi(\boldsymbol{y})[\boldsymbol{n}(\boldsymbol{y})\cdot\nabla_y\mathcal{G}(\boldsymbol{y},\boldsymbol{x})]dS(\boldsymbol{x}'), \tag{S12}$$

where $\mathcal{G}(\boldsymbol{y},\boldsymbol{x})$ is the Green's function for the potential at $\boldsymbol{y}$ due to a point charge at $\boldsymbol{x}$, and the surface S is made up of two contributions: one enclosing the particle (S_p) and another spherical surface of large radius (S_∞). For a particle in an unbounded medium, the Green's function is

$$\mathcal{G}(\boldsymbol{y},\boldsymbol{x}) = \frac{1}{4\pi r}, \tag{S13}$$

where $\boldsymbol{r} = \boldsymbol{y} - \boldsymbol{x}$. We first consider the integrals over the spherical surface far from the particle,

$$-\int_{S_\infty} \mathcal{G}(\boldsymbol{y},\boldsymbol{x})[\boldsymbol{n}(\boldsymbol{y})\cdot\nabla\Phi^\infty(\boldsymbol{y})]dS(\boldsymbol{y}) = \int_{S_\infty} \frac{1}{4\pi r}[\boldsymbol{n}(\boldsymbol{y})\cdot\boldsymbol{E}^\infty]dS(\boldsymbol{y}) = -\frac{1}{3}\boldsymbol{x}\cdot\boldsymbol{E}^\infty, \tag{S14}$$

$$\int_{S_\infty} \Phi^\infty(\boldsymbol{y})[\boldsymbol{n}(\boldsymbol{y})\cdot\nabla_y\mathcal{G}(\boldsymbol{y},\boldsymbol{x})]dS(\boldsymbol{y}) = \int_{S_\infty} (\boldsymbol{y}\cdot\boldsymbol{E}^\infty)\frac{\boldsymbol{n}(\boldsymbol{y})\cdot\boldsymbol{r}}{4\pi r^3}dS(\boldsymbol{y}) = -\frac{2}{3}\boldsymbol{x}\cdot\boldsymbol{E}^\infty. \tag{S15}$$

Substituting this result, we obtain

$$\frac{1}{2}\Phi(\boldsymbol{x}) = \Phi^\infty(\boldsymbol{x}) - \int_{S_p} \mathcal{G}(\boldsymbol{y},\boldsymbol{x})[\boldsymbol{n}(\boldsymbol{y})\cdot\nabla\Phi(\boldsymbol{y})]dS(\boldsymbol{y}) + \int_{S_p} \Phi(\boldsymbol{y})[\boldsymbol{n}(\boldsymbol{y})\cdot\nabla_y\mathcal{G}(\boldsymbol{y},\boldsymbol{x})]dS(\boldsymbol{y}). \tag{S16}$$

The first integral is identically zero owing to the boundary condition (S10). Substituting the Green's function, we obtain the following integral equation for the unknown potential on the surface of the particle

$$\frac{1}{2}\Phi(\boldsymbol{x}) = \Phi^\infty(\boldsymbol{x}) - \int_{S_p} \Phi(\boldsymbol{y})\frac{\boldsymbol{n}(\boldsymbol{y})\cdot\boldsymbol{r}}{4\pi r^3}dS(\boldsymbol{y}). \tag{S17}$$

As this integral is weakly singular, it is helpful to regularize it using integral identities [2] to obtain

$$\Phi(\boldsymbol{x}) = \Phi^\infty(\boldsymbol{x}) - \int_{S_p} [\Phi(\boldsymbol{y}) - \Phi(\boldsymbol{x})]\frac{\boldsymbol{n}(\boldsymbol{y})\cdot\boldsymbol{r}}{4\pi r^3}dS(\boldsymbol{y}). \tag{S18}$$

The implementation of this integral equation is detailed in Section 3.4 below.

3.2.2 Integral Equation for the Potential Gradient $\nabla\Phi(\boldsymbol{x})$

Differentiating equation (S17), we obtain

$$\frac{1}{2}\frac{\partial\Phi}{\partial x_i} = \frac{\partial\Phi^\infty}{\partial x_i} + \int_{S_p} \Phi(\boldsymbol{y})n_j(\boldsymbol{y})\frac{\partial^2\mathcal{G}(\boldsymbol{y},\boldsymbol{x})}{\partial x_i\partial y_j}dS(\boldsymbol{y}), \tag{S19}$$

where the relevant Green's function derivative is

$$\frac{\partial^2\mathcal{G}(\boldsymbol{y},\boldsymbol{x})}{\partial x_i\partial y_j} = \frac{1}{4\pi}\left(\frac{\delta_{ij}}{r^3} - \frac{3r_ir_j}{r^5}\right). \tag{S20}$$

Here, we are only interested in those components of the potential gradient that are tangent to the surface of the particle ($\boldsymbol{t}\cdot\nabla\Phi$); the component normal to the surface is identically zero in accordance with boundary condition (S10). This integral is hypersingular, but can be regularized using integral identities to obtain the following weakly singular integral equation for the potential gradient

$$\frac{1}{2}\frac{\partial\Phi}{\partial x_i} = \frac{\partial\Phi^\infty}{\partial x_i} + \int_{S_p} [\Phi(\boldsymbol{y}) - \Phi(\boldsymbol{x})]n_j(\boldsymbol{y})\frac{\partial^2\mathcal{G}(\boldsymbol{y},\boldsymbol{x})}{\partial x_i\partial y_j}dS(\boldsymbol{y}). \tag{S21}$$

3.3 Hydrodynamics

The fluid flows outside of the particle are described by the Stokes equations for creeping flow

$$\nabla \cdot \boldsymbol{\sigma} = -\nabla p + \eta \nabla^2 \boldsymbol{u} = 0 \quad \text{and} \quad \nabla \cdot \boldsymbol{u} = 0, \tag{S22}$$

where $\boldsymbol{u}(\boldsymbol{x})$ is the velocity, $p(\boldsymbol{x})$ is the pressure, $\boldsymbol{\sigma}(\boldsymbol{x})$ is the stress, and η is the viscosity. The particle moves as a rigid body with a translational velocity $\boldsymbol{U}$ and angular velocity $\boldsymbol{\Omega}$. Here, we adopt a moving frame of reference centered on the particle. In this frame, there is no flow normal to the particle surface

$$\boldsymbol{n} \cdot \boldsymbol{u} = 0 \text{ for } \boldsymbol{x} \in S_p. \tag{S23}$$

The force of the electric field on the field-induced double layer induces a slip velocity tangential to the particle surface

$$\boldsymbol{t} \cdot \boldsymbol{u} = \boldsymbol{t} \cdot \boldsymbol{u}_s = \boldsymbol{t} \cdot \left(\frac{\varepsilon}{\eta} \zeta(\boldsymbol{x}) \nabla \Phi(\boldsymbol{x}) \right) \text{ for } \boldsymbol{x} \in S_p, \tag{S24}$$

where $\boldsymbol{t}$ is a unit vector tangent to the surface, and $\zeta(\boldsymbol{x})$ is the spatially dependent zeta potential. Here, $\zeta(\boldsymbol{x}) = C - \Phi(\boldsymbol{x})$ where C is a constant chosen such that surface averaged zeta potential is zero. Far from the particle, the velocity approaches the rigid body velocity

$$\boldsymbol{u}(\boldsymbol{x}) = \boldsymbol{u}^{\infty}(\boldsymbol{x}) = -(\boldsymbol{U} + \boldsymbol{\Omega} \times \boldsymbol{x}) \text{ for } \boldsymbol{x} \to \infty. \tag{S25}$$

The translation and rotational velocities are determined by the constraints that there is no net force or torque acting on the particle

$$\int_{S_p} \boldsymbol{f}(\boldsymbol{y}) dS(\boldsymbol{y}) = 0, \tag{S26}$$

$$\int_{S_p} \boldsymbol{y} \times \boldsymbol{f}(\boldsymbol{y}) dS(\boldsymbol{y}) = 0, \tag{S27}$$

where $\boldsymbol{f} = \boldsymbol{\sigma} \cdot \boldsymbol{n}$ is the stress on the surface. Rather than solve this problem directly, it is convenient to make use of the Lorentz reciprocal theorem to obtain [3, 4]

$$\hat{\boldsymbol{F}} \cdot \boldsymbol{U} + \hat{\boldsymbol{L}} \cdot \boldsymbol{\Omega} = -\int_{S_p} \boldsymbol{u}_s(\boldsymbol{y}) \cdot \hat{\boldsymbol{f}}(\boldsymbol{y}) dS(\boldsymbol{y}), \tag{S28}$$

where $\hat{\boldsymbol{f}} = \hat{\boldsymbol{\sigma}} \cdot \boldsymbol{n}$ is the stress due to the same particle undergoing pure translational or rotational motion through a quiescent fluid. The associated force $\hat{\boldsymbol{F}}$ and torque $\hat{\boldsymbol{L}}$ are given by

$$\hat{\boldsymbol{F}} = \int_{S_p} \hat{\boldsymbol{f}}(\boldsymbol{y}) dS(\boldsymbol{y}) \quad \text{and} \quad \hat{\boldsymbol{T}} = \int_{S_p} \boldsymbol{y} \times \hat{\boldsymbol{f}}(\boldsymbol{y}) dS(\boldsymbol{y}). \tag{S29}$$

3.3.1 Integral Equation for the Stress $\hat{\boldsymbol{f}}(\boldsymbol{x})$

To obtain the stress $\hat{\boldsymbol{f}}(\boldsymbol{x})$ for the associated Stokes flow due to simple translational/rotational motion, we start from the integral equation for the velocity at a point $\boldsymbol{x}$ on the surface of the particle [2]

$$\frac{1}{2} \hat{u}_j(\boldsymbol{x}) = -\frac{1}{\eta} \int_S \mathcal{G}_{ij}(\boldsymbol{y}, \boldsymbol{x}) \hat{f}_i(\boldsymbol{y}) dS(\boldsymbol{y}) + \int_S \hat{u}_i(\boldsymbol{y}) \mathcal{T}_{ijk}(\boldsymbol{y}, \boldsymbol{x}) n_k(\boldsymbol{y}) dS(\boldsymbol{y}), \tag{S30}$$

where the free-space Green's functions are given by

$$\mathcal{G}_{ij}(\boldsymbol{y}, \boldsymbol{x}) = \frac{1}{8\pi} \left(\frac{\delta_{ij}}{r} + \frac{r_i r_j}{r^3} \right), \tag{S31}$$

$$\mathcal{T}_{ijk}(\boldsymbol{y}, \boldsymbol{x}) = -\frac{3 r_i r_j r_k}{4\pi r^5}, \tag{S32}$$

with $r_i = y_i - x_i$ as above. As in the electrostatics problem, the surface S is made up of two parts: one closely enclosing the particle (S_p), the other a spherical surface of large radius (S_∞). Evaluating analytically the integrals over the outer surface and noting that the surface velocity is zero, we obtain

$$\frac{1}{2}\hat{u}_j(\boldsymbol{x}) = \hat{u}_j^\infty(\boldsymbol{x}) - \frac{1}{\eta}\int_{S_p} \mathcal{G}_{ij}(\boldsymbol{y},\boldsymbol{x})\hat{f}_i(\boldsymbol{y})dS(\boldsymbol{y}), \tag{S33}$$

where the velocity far from the particle is due to pure translation and/or rotation

$$\hat{\boldsymbol{u}}^\infty(\boldsymbol{x}) = -(\hat{\boldsymbol{U}} + \hat{\boldsymbol{\Omega}} \times \boldsymbol{x}) \text{ for } \boldsymbol{x} \to \infty. \tag{S34}$$

Equation (S33) can then be solved numerically for the unknown surface stress, $\hat{\boldsymbol{f}}(\boldsymbol{x})$ (see below).

3.4 Numerical Solution

3.4.1 Lebedev Quadrature

The integral equations above are solved numerically using Lebedev quadrature [5] over surfaces parameterized by the spherical angles θ and ϕ. In this approach, integrals are approximated as

$$\int_0^{2\pi}\int_0^{\pi} g(\theta,\phi)\sin\theta d\theta\ d\phi \approx \sum_{q=1}^{N} w_q g(\theta_q,\phi_q), \tag{S35}$$

where the grid points (θ_q, ϕ_q) have octahedral rotation and inversion symmetry, and the grid weights w_i enable the exact integration of spherical harmonics up to a given order. To compute a surface integral over the parametric particle surface $\boldsymbol{x}(\theta,\phi)$, we can write

$$\int_{S_p} g(\boldsymbol{x})dS = \int_0^{\pi}\int_0^{2\pi} g(\theta,\phi)|\boldsymbol{x}_\theta \times \boldsymbol{x}_\phi| d\phi d\theta \approx \sum_{q=1}^{N} W_q g(\theta_q,\phi_q), \tag{S36}$$

where the weighting factor W_q contains both the Lebedev weights and the surface area element

$$W_q = \frac{w_q}{\sin\theta_q}|\boldsymbol{x}_\theta \times \boldsymbol{x}_\phi|_q. \tag{S37}$$

3.4.2 Electrostatics

To circumvent the challenges associated with the singular integrand in equation (S18), we introduce an alternative Green-like function $\mathcal{G}_\alpha(\boldsymbol{y},\boldsymbol{x})$ for the potential at point $\boldsymbol{y}$ due to a Gaussian charge distribution of width $\alpha^{1/2}$ centered at point $\boldsymbol{x}$

$$\mathcal{G}_\alpha(\boldsymbol{y},\boldsymbol{x}) = \int_V \frac{e^{-\pi r''^2/\alpha}}{\alpha^{3/2}}\mathcal{G}(\boldsymbol{y},\boldsymbol{x}')d\boldsymbol{x}' = \frac{1}{4\pi r}\,\mathrm{erf}\left(\sqrt{\pi r^2/\alpha}\right), \tag{S38}$$

where $\boldsymbol{r} = \boldsymbol{y} - \boldsymbol{x}$ and $\boldsymbol{r}'' = \boldsymbol{x}' - \boldsymbol{x}$. This function approaches that of equation (S13) in the limit as $\alpha \to 0$. The integral equation (S17) for the potential can now be recast as

$$\begin{aligned}\Phi(\boldsymbol{x}) = \Phi^\infty(\boldsymbol{x}) &+ \int_{S_p}[\Phi(\boldsymbol{y}) - \Phi(\boldsymbol{x})]\boldsymbol{n}(\boldsymbol{y})\cdot\nabla_y\mathcal{G}_\alpha(\boldsymbol{y},\boldsymbol{x})dS(\boldsymbol{y}) + \\ &+ \int_{S_p}[\Phi(\boldsymbol{y}) - \Phi(\boldsymbol{x})]\boldsymbol{n}(\boldsymbol{y})\cdot\nabla_y\left[\mathcal{G}(\boldsymbol{y},\boldsymbol{x}) - \mathcal{G}_\alpha(\boldsymbol{y},\boldsymbol{x})\right]dS(\boldsymbol{y}).\end{aligned} \tag{S39}$$

The first integral is non-singular and can be computed numerically by Lebedev quadrature. The second integral is non-zero only in the vicinity of the singularity (i.e., when $|\boldsymbol{y}-\boldsymbol{x}| \sim \alpha^{1/2}$) and can be approximated analytically as

$$\int_{S_p}[\Phi(\boldsymbol{y}) - \Phi(\boldsymbol{x})]\boldsymbol{n}(\boldsymbol{y})\cdot\nabla_y\left[\mathcal{G}(\boldsymbol{y},\boldsymbol{x}) - \mathcal{G}_\alpha(\boldsymbol{y},\boldsymbol{x})\right]dS(\boldsymbol{y}) = 0 + O(\alpha^{3/2}), \tag{S40}$$

where we neglect all contributions of order $\alpha^{3/2}$ and higher.

The potential gradient tangent to the surface can be computed in similar fashion. We first decompose equation (S19) for the potential gradient into "far-field" and "near-field" components as

$$\begin{aligned}\frac{1}{2}t_i(\boldsymbol{x})\frac{\partial\Phi(\boldsymbol{x})}{\partial x_i} = t_i(\boldsymbol{x})\frac{\partial\Phi^{\infty}(\boldsymbol{x})}{\partial x_i} + \int_{S_p}\left[\Phi(\boldsymbol{y})-\Phi(\boldsymbol{x})\right]t_i(\boldsymbol{x})n_j(\boldsymbol{y})\frac{\partial^2\mathcal{G}_\alpha(\boldsymbol{y},\boldsymbol{x})}{\partial x_i\partial y_j}dS(\boldsymbol{y}) + \\ + \int_{S_p}\left[\Phi(\boldsymbol{y})-\Phi(\boldsymbol{x})\right]t_i(\boldsymbol{x})n_j(\boldsymbol{y})\frac{\partial^2\left[\mathcal{G}(\boldsymbol{y},\boldsymbol{x})-\mathcal{G}_\alpha(\boldsymbol{y},\boldsymbol{x})\right]}{\partial x_i\partial y_j}dS(\boldsymbol{y}),\end{aligned} \tag{S41}$$

where the former is handled numerically and the later analytically. Specifically, the "near-field" component is approximated as

$$\int_{S_p}\left[\Phi(\boldsymbol{y})-\Phi(\boldsymbol{x})\right]t_i(\boldsymbol{x})n_j(\boldsymbol{y})\frac{\partial^2\left[\mathcal{G}(\boldsymbol{y},\boldsymbol{x})-\mathcal{G}_\alpha(\boldsymbol{y},\boldsymbol{x})\right]}{\partial x_i\partial y_j}dS(\boldsymbol{y}) = t_i(\boldsymbol{x})\frac{\partial\Phi(\boldsymbol{x})}{\partial x_i}\frac{H(\boldsymbol{x})\alpha^{1/2}}{2\pi} + O(\alpha^{3/2}), \tag{S42}$$

where $H(\boldsymbol{x})$ is the mean curvature of the surface.

3.4.3 Hydrodynamics

As in the electrostatics problem, we divide the integrals of equation (S33) into near-field and far-field components as

$$\frac{1}{2}\hat{u}_j(\boldsymbol{x}) = \hat{u}_j^{\infty}(\boldsymbol{x}) - \frac{1}{\eta}\int_S \mathcal{G}_{ij}^{\alpha}(\boldsymbol{y},\boldsymbol{x})\hat{f}_i(\boldsymbol{y})dS(\boldsymbol{y}) - \frac{1}{\eta}\int_S\left[\mathcal{G}_{ij}(\boldsymbol{y},\boldsymbol{x})-\mathcal{G}_{ij}^{\alpha}(\boldsymbol{y},\boldsymbol{x})\right]\hat{f}_i(\boldsymbol{y})dS(\boldsymbol{y}). \tag{S43}$$

Here, the function $\mathcal{G}_{ij}^{\alpha}(\boldsymbol{y},\boldsymbol{x})$ represents the Green's function for the velocity modulated by a Gaussian filter of the form described in [6]

$$\begin{aligned}\mathcal{G}_{ij}^{\alpha}(\boldsymbol{y},\boldsymbol{x}) &= \int_V \frac{e^{-\pi r''^2/\alpha}}{\alpha^{3/2}}\left(\frac{5}{2}-\frac{\pi r''^2}{\alpha}\right)\mathcal{G}_{ij}(\boldsymbol{y},\boldsymbol{x}')d\boldsymbol{x}', \\ &= \frac{1}{8\pi}\left[\left(\operatorname{erf}\left(\sqrt{\pi r^2/\alpha}\right)+\frac{2re^{-\pi r^2/\alpha}}{\alpha^{1/2}}\right)\frac{\delta_{ij}}{r} + \left(\operatorname{erf}\left(\sqrt{\pi r^2/\alpha}\right)-\frac{2re^{-\pi r^2/\alpha}}{\alpha^{1/2}}\right)\frac{r_ir_j}{r^3}\right],\end{aligned} \tag{S44}$$

where $\boldsymbol{r} = \boldsymbol{y}-\boldsymbol{x}$ and $\boldsymbol{r}'' = \boldsymbol{x}'-\boldsymbol{x}$. The far-field contribution (first integral) can be computed numerically without singularities; the near-field contribution (second integral) can be approximated analytically as

$$-\frac{1}{\eta}\int_{S_p}\left[\mathcal{G}_{ij}(\boldsymbol{y},\boldsymbol{x})-\mathcal{G}_{ij}^{\alpha}(\boldsymbol{y},\boldsymbol{x})\right]\hat{f}_i(\boldsymbol{y})dS(\boldsymbol{y}) = -\frac{\alpha^{1/2}}{4\pi\eta}\left[\delta_{ij}-n_i(\boldsymbol{x})n_j(\boldsymbol{x})\right]\hat{f}_i(\boldsymbol{x}) + O(\alpha^{3/2}). \tag{S45}$$

3.4.4 Error Analysis

To validate the numerical method detailed above, we consider the problem of a spherical particle, for which the exact solutions to the electrostatic and hydrodynamic problems are known. Figure (S2) shows the error in the dipole moment as a function of the Gaussian width α and the number of Lebedev grid points N. For a given Gaussian width α, the number of Lebedev points required to converge to a stable solution (independent of N) is $N \sim 4\pi a^2/\alpha$. Thus, the smaller the Gaussian width, the more grid points are required to accurately solve the integral equations. When N is sufficiently large ($N \gg 4\pi a^2/\alpha$), the primary source of error derives from the analytical approximation of equation (S40), which neglected contributions of order $\alpha^{3/2}$ and higher. Consequently, the error in the dipole moment (and all other electrostatic quantities) scales as $\alpha^{3/2}$ with the Gaussian width and thereby as $N^{-3/2}$ with the number of Lebedev grid points. Figure (S3) shows a similar analysis of the root mean square (RMS) velocity on the surface of a sphere.

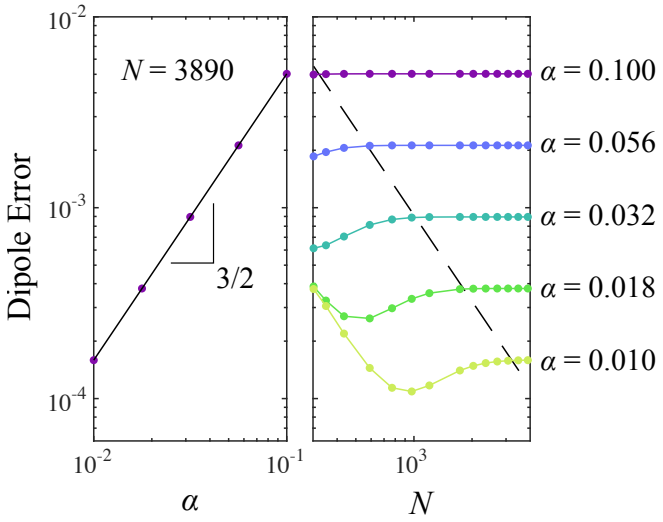

Figure S2: Numerical error in computing the dipole moment of a conductive sphere in a uniform electric field as a function of the Gaussian peak width α (left) and the number of Lebedev points N (right). The dipole error is presented in natural units of $\varepsilon a^3 E^\infty$; the exact dipole moment for a sphere is 2π.

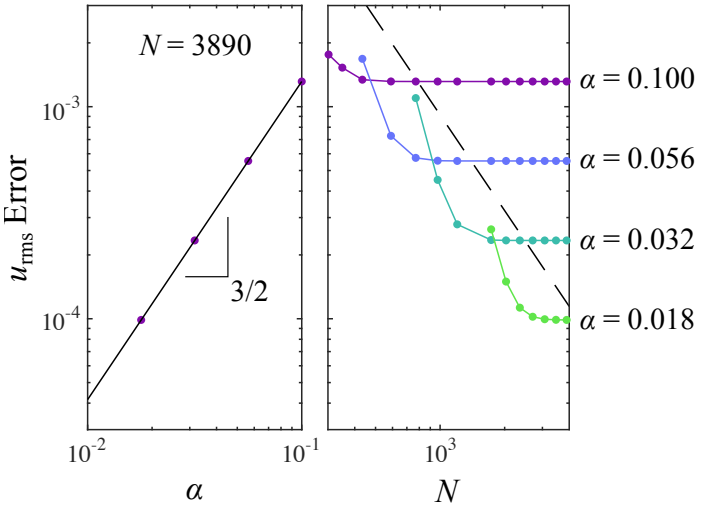

Figure S3: Numerical error in computing the RMS velocity on the surface of a conductive sphere in a uniform electric field as a function of the Gaussian peak width α (left) and the number of Lebedev points N (right). The velocity error is presented in natural units of $\varepsilon a {E^\infty}^2/\eta$; the exact RMS surface velocity for a sphere is $\frac{3}{2}\sqrt{3/10}$.

4 Particle Dynamics

4.1 $D_{\infty h}$ Rotation Class

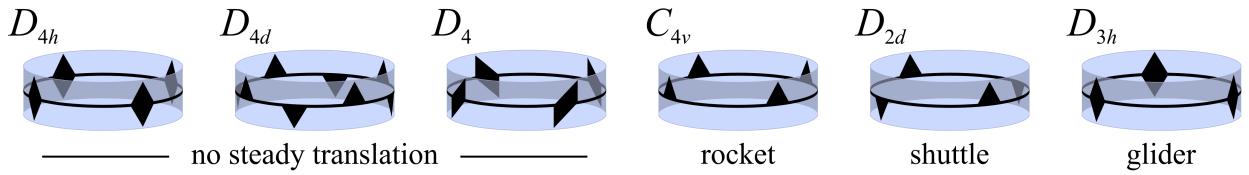

Figure S4: Schematic illustration of symmetry groups included in the $D_{\infty h}$ rotation class; point groups with $n = 4$ are representative of all particles with $n \geq 4$. Particles with these symmetries exhibit the same rotational motions but differ in their translational motions.

Rotational Dynamics

The rotation tensor in the particle frame $\mathfrak{D}'_{ijk}$ has only one parameter: $-\mathfrak{D}'_{123} = -\mathfrak{D}'_{132} = \mathfrak{D}'_{213} = \mathfrak{D}'_{231} = d$. By convention, the primary axis of the particle is oriented along the z'-direction. To help to visualize the structure of $\mathfrak{D}'$, we will write it explicitly as

$$\mathfrak{D}' = \begin{bmatrix} \begin{pmatrix} 0 & 0 & 0 \\ 0 & 0 & d \\ 0 & 0 & 0 \end{pmatrix} & \begin{pmatrix} 0 & 0 & -d \\ 0 & 0 & 0 \\ 0 & 0 & 0 \end{pmatrix} & \begin{pmatrix} 0 & -d & 0 \\ d & 0 & 0 \\ 0 & 0 & 0 \end{pmatrix} \end{bmatrix}. \tag{S46}$$

The equations of motion expressed using Euler angles (ϕ, θ, ψ) simplify to

$$\begin{aligned} \dot{\phi} &= 0, \\ \dot{\theta} &= -d \sin 2\theta, \\ \dot{\psi} &= 0. \end{aligned} \tag{S47}$$

These equations admit the following stable fixed points

$$\begin{aligned} \theta &= m\pi \text{ for } d > 0, \\ \theta &= (m + \tfrac{1}{2})\pi \text{ for } d < 0, \end{aligned} \tag{S48}$$

with $m \in$ integers. Physically, the particle adopts a stable orientation with its longer axis aligned parallel to the applied field. These dynamics are conveniently summarized by the phase portraits of Figure S5 for positive and negative d. The parameter d provides a convenient measure of the effective aspect ratio of the particle.

C_{nv} Particles ($n \geq 4$): Rockets

The translation tensor in the particle frame $\mathfrak{C}'_{ijk}$ has three parameters: $\mathfrak{C}'_{333} = c_1$, $\mathfrak{C}'_{311} = \mathfrak{C}'_{322} = c_2$, and $\mathfrak{C}'_{113} = \mathfrak{C}'_{131} = \mathfrak{C}'_{223} = \mathfrak{C}'_{232} = c_3$,

$$\mathfrak{C}' = \begin{bmatrix} \begin{pmatrix} 0 & 0 & c_3 \\ 0 & 0 & 0 \\ c_2 & 0 & 0 \end{pmatrix} & \begin{pmatrix} 0 & 0 & 0 \\ 0 & 0 & c_3 \\ 0 & c_2 & 0 \end{pmatrix} & \begin{pmatrix} c_3 & 0 & 0 \\ 0 & c_3 & 0 \\ 0 & 0 & c_1 \end{pmatrix} \end{bmatrix}. \tag{S49}$$

As above, the primary axis of the particle is oriented along the z'-direction. When the axis of the particle is oriented parallel to the applied field, the velocity is c_1 in the z'-direction. When the axis is perpendicular to the field, the velocity is c_2 in the z'-direction. The parameter c_3 is needed only to describe transient particle motions during its rotation into the stable orientation.

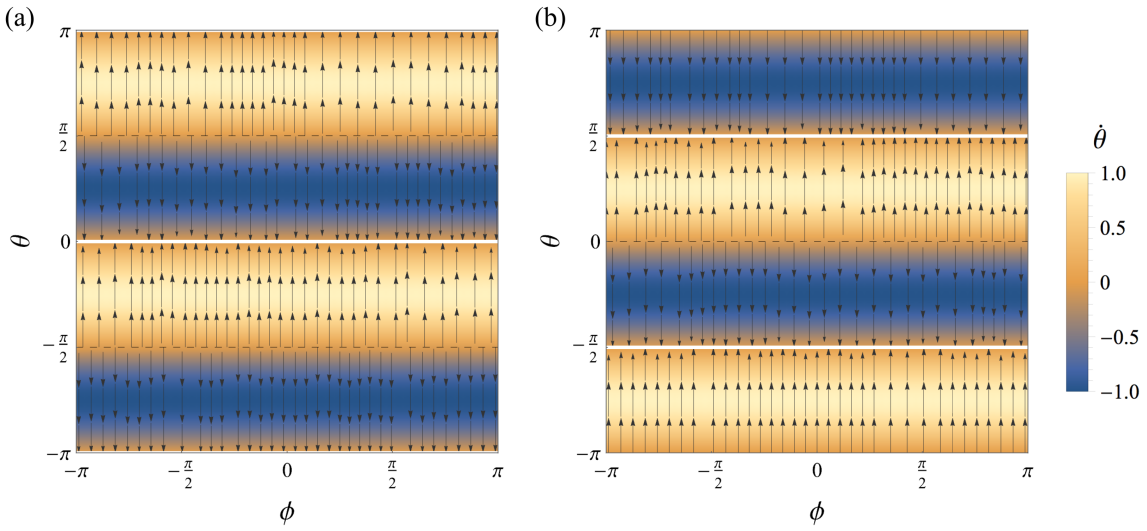

Figure S5: Phase portraits for the $D_{\infty h}$ class for (a) $d = 1$ and (b) $d = -1$. The colormap shows the magnitude of $\dot{\theta}$; arrows show the flow in the $\phi\theta$ plane. The line of stable fixed points is marked by the white curves.

D_{2d} Particles: Shuttles

The translation tensor in the particle frame $\mathfrak{C}'_{ijk}$ has two parameters: $\mathfrak{C}'_{321} = \mathfrak{C}'_{312} = c_1$ and $\mathfrak{C}'_{132} = \mathfrak{C}'_{123} = \mathfrak{C}'_{213} = \mathfrak{C}'_{231} = c_2$,

$$\mathfrak{C}' = \begin{bmatrix} \begin{pmatrix} 0 & 0 & 0 \\ 0 & 0 & c_2 \\ 0 & c_1 & 0 \end{pmatrix} & \begin{pmatrix} 0 & 0 & c_2 \\ 0 & 0 & 0 \\ c_1 & 0 & 0 \end{pmatrix} & \begin{pmatrix} 0 & c_2 & 0 \\ c_2 & 0 & 0 \\ 0 & 0 & 0 \end{pmatrix} \end{bmatrix}. \tag{S50}$$

As above, the primary C_2 axis of the particle is oriented along the z'-direction; the particle is further rotated about that axis such that its $C_{2'}$ axes lie along the x' and y' directions. When the axis of the particle is oriented parallel to the applied field, the velocity is zero. When the axis is perpendicular to the field, the velocity is $2c_1 \cos\phi \sin\phi$ in the z'-direction (along the particle axis). The parameter c_2 is needed only to describe transient particle motions during its rotation into the stable orientation.

D_{3h} Particles: Gliders

The translation tensor in the particle frame $\mathfrak{C}'_{ijk}$ has one parameter: $-\mathfrak{C}'_{123} = -\mathfrak{C}'_{132} = \mathfrak{C}'_{213} = \mathfrak{C}'_{231} = c.$,

$$\mathfrak{C}' = \begin{bmatrix} \begin{pmatrix} -c & 0 & 0 \\ 0 & c & 0 \\ 0 & 0 & 0 \end{pmatrix} & \begin{pmatrix} 0 & c & 0 \\ c & 0 & 0 \\ 0 & 0 & 0 \end{pmatrix} & \begin{pmatrix} 0 & 0 & 0 \\ 0 & 0 & 0 \\ 0 & 0 & 0 \end{pmatrix} \end{bmatrix}. \tag{S51}$$

Here, the primary axis of the particle is oriented along the z'-direction; the particle is further rotated about that axis such that one of its three C_2 rotation axes lies along the x'-direction. When the axis of the particle is oriented parallel to the applied field, its velocity is zero. When the axis is perpendicular to the field such that its z' axis lies along the y-direction (i.e., $\theta = \psi = 0$), the particle moves perpendicular to its axis in the xz-plane with velocity $\boldsymbol{U} = c[\cos(3\phi)\boldsymbol{e}_x + \sin(3\phi)\boldsymbol{e}_z]$. The direction of translation depends on the orientation of the particle about its axis (i.e., on ϕ).

D_n Particles ($n \geq 4$)

The translation tensor in the particle frame $\mathfrak{C}'_{ijk}$ has one parameter: $-\mathfrak{C}'_{111} = \mathfrak{C}'_{122} == \mathfrak{C}'_{212} == \mathfrak{C}'_{221} = c$,

$$\mathfrak{C}' = \begin{bmatrix} \begin{pmatrix} 0 & 0 & 0 \\ 0 & 0 & c \\ 0 & 0 & 0 \end{pmatrix} & \begin{pmatrix} 0 & 0 & -c \\ 0 & 0 & 0 \\ 0 & 0 & 0 \end{pmatrix} & \begin{pmatrix} 0 & -c & 0 \\ c & 0 & 0 \\ 0 & 0 & 0 \end{pmatrix} \end{bmatrix} . \tag{S52}$$

Here, the primary axis of the particle is oriented along the z'-direction. When the axis of the particle is oriented parallel or perpendicular to the applied field, its velocity is zero. However, the particles exhibits transient translational motions with speed c as its axis approaches its stable orientation.

4.2 D_{2h} Rotation Class

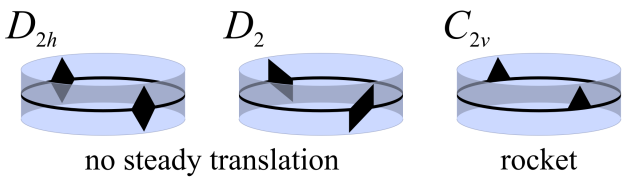

Figure S6: Schematic illustration of symmetry groups included in the D_{2h} rotation class. Particles with these symmetries exhibit the same rotational motions but differ in their translational motions.

Rotational Dynamics

The rotation tensor $\mathfrak{D}'_{ijk}$ has the following non-zero elements: $\mathfrak{D}'_{123} = \mathfrak{D}'_{132}$, $\mathfrak{D}'_{213} = \mathfrak{D}'_{231}$, and $\mathfrak{D}'_{312} = \mathfrak{D}'_{321}$. By convention, the principal axes of the particle are aligned along the x', y', and z'-directions. The D_{2h} rotation tensor can be constructed by superimposing three $D_{\infty h}$ tensors oriented along the x', y', and z'-axes and parameterized by d_1, d_2, and d_3, respectively,

$$\mathfrak{D}' = \begin{bmatrix} \begin{pmatrix} 0 & 0 & 0 \\ 0 & 0 & d_3 - d_1 \\ 0 & d_1 - d_2 & 0 \end{pmatrix} & \begin{pmatrix} 0 & 0 & d_2 - d_3 \\ 0 & 0 & 0 \\ d_1 - d_2 & 0 & 0 \end{pmatrix} & \begin{pmatrix} 0 & d_2 - d_3 & 0 \\ d_3 - d_1 & 0 & 0 \\ 0 & 0 & 0 \end{pmatrix} \end{bmatrix}. \tag{S53}$$

By convention, the particle frame is chosen such that $d_1 \leq d_2 \leq d_3$. The equations of motion expressed using Euler angles simplify to

$$\begin{aligned} \dot{\phi} &= (d_1 - d_2) \sin 2\phi, \\ \dot{\theta} &= \tfrac{1}{2}[d_1 + d_2 - 2d_3 + (d_2 - d_1) \cos 2\phi] \sin 2\theta, \\ \dot{\psi} &= (d_2 - d_1) \sin 2\phi \cos\theta. \end{aligned} \tag{S54}$$

For $d_1 < d_2 < d_3$, these equations admit stable fixed points at

$$\phi = n\pi \text{ and } \theta = m\pi, \tag{S55}$$

for integers n and m. Physically, the particle adopts a stable orientation with the longest of its principal axes aligned parallel to the field.

C_{2v} Particles: Rockets

The translation tensor in the particle frame $\mathfrak{C}'_{ijk}$ has five parameters: $\mathfrak{C}'_{333} = c_1$, $\mathfrak{C}'_{322} = c_2$, $\mathfrak{C}'_{311} = c_3$, $\mathfrak{C}'_{223} = \mathfrak{C}'_{232} = c_4$, and $\mathfrak{C}'_{113} = \mathfrak{C}'_{131} = c_5$,

$$\mathfrak{C}' = \begin{bmatrix} \begin{pmatrix} 0 & 0 & c_5 \\ 0 & 0 & 0 \\ c_3 & 0 & 0 \end{pmatrix} & \begin{pmatrix} 0 & 0 & 0 \\ 0 & 0 & c_4 \\ 0 & c_2 & 0 \end{pmatrix} & \begin{pmatrix} c_5 & 0 & 0 \\ 0 & c_4 & 0 \\ 0 & 0 & c_1 \end{pmatrix} \end{bmatrix}. \tag{S56}$$

As above, the primary axis of the particle is oriented along the z'-direction; the particle is further rotated about the z'-axis such that $d_1 \leq d_2$. When the axis of the particle is oriented parallel to the applied field (i.e., when $d_3 > d_2$), the velocity is c_1 in the z'-direction (along the particle axis). When the axis is perpendicular to the field such that its z' axis lies along the y-direction (i.e., $\theta = \psi = 0$), the particle moves parallel to its axis with velocity $\boldsymbol{U} = -(c_2 \cos^2\phi + c_3 \sin^2\phi)\boldsymbol{e}_y$. The parameters c_4 and c_5 are needed only to describe transient particle motions during its rotation into the stable orientation.

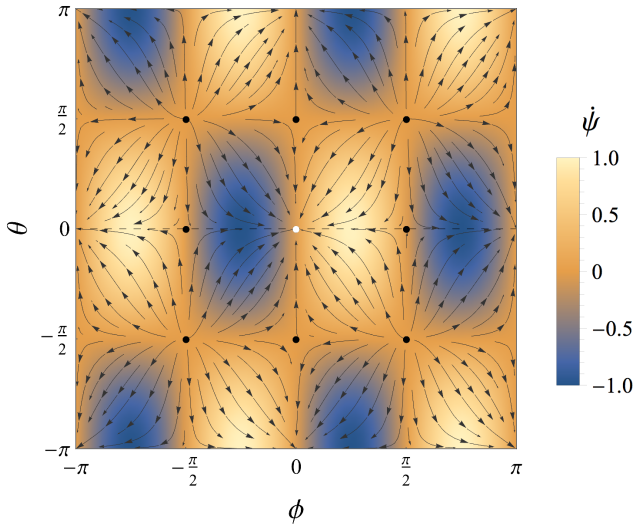

Figure S7: Phase portrait for the D_{2h} class for $d_1 = -1$, $d_2 = 0$, and $d_3 = 1$. The colormap shows the magnitude of $\dot{\psi}$; arrows show the flow in the $\phi\theta$ plane. The stable fixed point is marked by the white dot.

4.3 D_{3d} Rotation Class

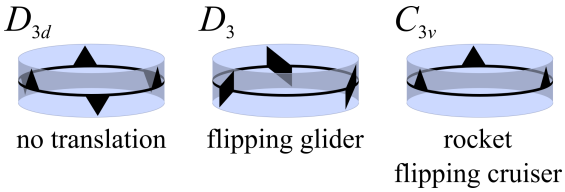

Figure S8: Schematic illustration of symmetry groups included in the D_{3d} rotation class. Particles with these symmetries exhibit the same rotational motions but differ in their translational motions.

Rotational Dynamics

The rotation tensor in the particle frame $\mathfrak{D}'_{ijk}$ can be expressed using two independent parameters: $-\mathfrak{D}'_{123} = -\mathfrak{D}'_{132} = \mathfrak{D}'_{213} = \mathfrak{D}'_{231} = d_1$ and $-\mathfrak{D}'_{111} = \mathfrak{D}'_{122} = \mathfrak{D}'_{212} = \mathfrak{D}'_{221} = d_2$.

$$\mathfrak{D}' = \begin{bmatrix} \begin{pmatrix} -d_2 & 0 & 0 \\ 0 & d_2 & d_1 \\ 0 & 0 & 0 \end{pmatrix} & \begin{pmatrix} 0 & d_2 & -d_1 \\ d_2 & 0 & 0 \\ 0 & 0 & 0 \end{pmatrix} & \begin{pmatrix} 0 & -d_1 & 0 \\ d_1 & 0 & 0 \\ 0 & 0 & 0 \end{pmatrix} \end{bmatrix}. \tag{S57}$$

Here, the particle is oriented such that its 3-fold rotation axis is aligned parallel to the z'-axis and one of its 2-fold rotation axes is aligned parallel to the x'-axis. The equations of motion expressed using Euler angles simplify to

$$\begin{aligned} \dot{\phi} &= -\tfrac{1}{2} d_2 (1 + 2\cos 2\phi) \sin\phi \sin 2\theta, \\ \dot{\theta} &= d_2 \cos 3\phi \sin^2\theta - d_1 \sin 2\theta, \\ \dot{\psi} &= d_2 (1 + 2\cos 2\phi) \sin\theta \sin\phi. \end{aligned} \tag{S58}$$

The dynamics have a fixed point at $\theta = m\pi$ for integer m, which corresponds to the particle's 3-fold rotation axis aligned parallel to the applied field; this orientation is stable when $d_1 > 0$. Alternatively, when $d_1 < 0$, the particle orients perpendicular to the applied field and rotates about the axis of the field. To summarize, the stable fixed points are

$$\begin{aligned} &\theta = m\pi, \quad \dot{\phi} = \dot{\psi} = 0 \quad \text{for} \quad d_1 > 0, \\ &\phi = (n + \tfrac{1}{2})\tfrac{\pi}{3}, \quad \theta = (m + \tfrac{1}{2})\pi, \quad \dot{\psi} = (-1)^{n+m} d_2 \quad \text{for } d_1 < 0. \end{aligned} \tag{S59}$$

Figure S9 illustrates phase portraits corresponding to these two different dynamical behaviors.

D_3 Particles: Flipping Gliders

The translation tensor in the particle frame $\mathfrak{C}'_{ijk}$ has two parameters: $-\mathfrak{C}'_{111} = \mathfrak{C}'_{122} = \mathfrak{C}'_{212} = \mathfrak{C}'_{221} = c_1$ and $-\mathfrak{C}'_{123} = -\mathfrak{C}'_{132} = \mathfrak{C}'_{213} = \mathfrak{C}'_{221} = c_2$,

$$\mathfrak{C}' = \begin{bmatrix} \begin{pmatrix} -c_1 & 0 & 0 \\ 0 & c_1 & c_2 \\ 0 & 0 & 0 \end{pmatrix} & \begin{pmatrix} 0 & c_1 & -c_2 \\ c_1 & 0 & 0 \\ 0 & 0 & 0 \end{pmatrix} & \begin{pmatrix} 0 & -c_2 & 0 \\ c_2 & 0 & 0 \\ 0 & 0 & 0 \end{pmatrix} \end{bmatrix}. \tag{S60}$$

As above, the particle is oriented such that its 3-fold rotation axis is aligned parallel to the z'-axis and one of its 2-fold rotation axes is aligned parallel to the x'-axis. When the axis of the particle is oriented parallel to the applied field (Figure S9a), there is no translational motion. When the axis is perpendicular to the field in its stable orientation (Figure S9b), the particle moves parallel to the field with speed c_1. The parameter c_2 is needed only to describe transient particle motions during its rotation into the stable orientation.

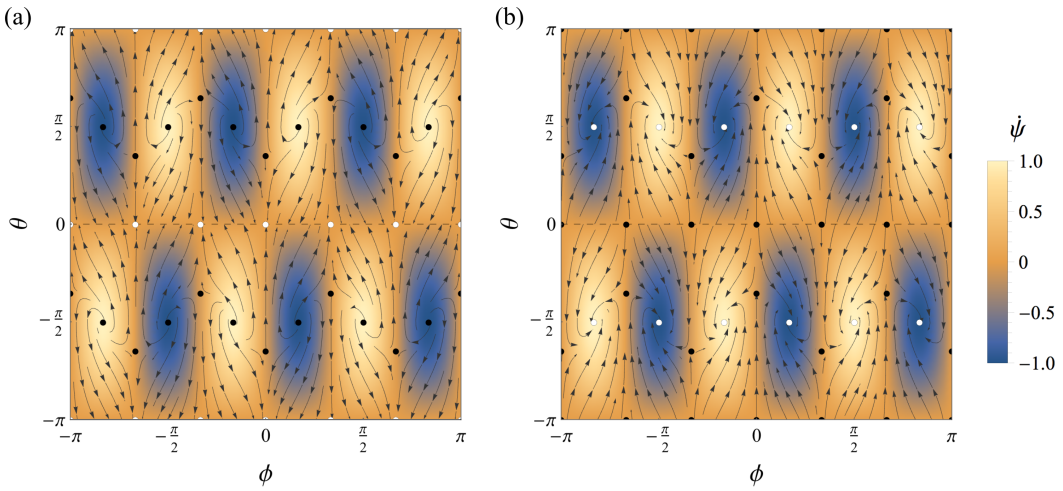

Figure S9: Phase portraits for the D_{3d} particle for (a) $d_1 = d_2 = 1$ and (b) $-d_1 = d_2 = 1$. The colormap shows the magnitude of $\dot{\psi}$; arrows show the flow in the $\phi\theta$ plane. Stable fixed points are marked by white circles; unstable by black circles.

C_{3v} Particles: Rockets / Flipping Cruisers

The translation tensor in the particle frame $\mathfrak{C}'_{ijk}$ has four parameters: $\mathfrak{C}'_{333} = c_1$, $\mathfrak{C}'_{311} = \mathfrak{C}'_{322} = c_2$, $-\mathfrak{C}'_{121} = -\mathfrak{C}'_{112} = -\mathfrak{C}'_{211} = \mathfrak{C}'_{222} = c_3$, and $\mathfrak{C}'_{131} = \mathfrak{C}'_{113} = \mathfrak{C}'_{232} = \mathfrak{C}'_{223} = c_4$,

$$\mathfrak{C}' = \begin{bmatrix} \begin{pmatrix} 0 & -c3 & c_4 \\ -c_3 & 0 & 0 \\ c_2 & 0 & 0 \end{pmatrix} & \begin{pmatrix} -c_3 & 0 & 0 \\ 0 & c_3 & c_4 \\ 0 & c_2 & 0 \end{pmatrix} & \begin{pmatrix} c_4 & 0 & 0 \\ 0 & c_4 & 0 \\ 0 & 0 & c_1 \end{pmatrix} \end{bmatrix}. \tag{S61}$$

The particle is oriented such that its 3-fold rotation axis is aligned parallel to the z'-axis and one of its planes of reflection symmetry is normal to the x'-axis. When the axis of the particle is oriented parallel to the applied field (Figure S9a), the particle moves parallel to the field with speed c_1. When the axis is perpendicular to the field in its stable orientation (Figure S9b), the particle moves perpendicular to the field with speed $\sqrt{c_2^2 + c_3^2}$. The parameter c_4 is needed only to describe transient particle motions during its rotation into the stable orientation.

4.4 C_{4h} Rotation Class

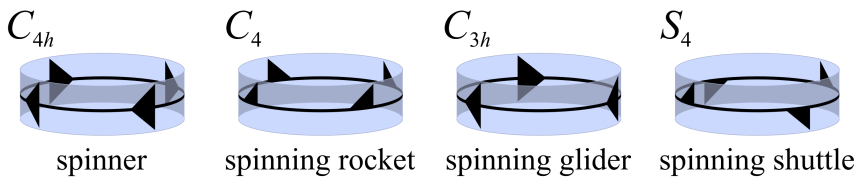

Figure S10: Schematic illustration of symmetry groups included in the C_{4h} rotation class; point groups with $n = 4$ are representative of all particles with $n \geq 4$. Particles with these symmetries exhibit the same rotational motions but differ in their translational motions.

Rotational Dynamics

The rotation tensor in the particle frame $\mathfrak{D}'_{ijk}$ can be expressed using four independent parameters: $-\mathfrak{D}'_{123} = -\mathfrak{D}'_{132} = \mathfrak{D}'_{213} = \mathfrak{D}'_{231} = d_1$, $\mathfrak{D}'_{333} = d_2$, $\mathfrak{D}'_{311} = \mathfrak{D}'_{322} = d_3$, and $\mathfrak{D}'_{113} = \mathfrak{D}'_{131} = \mathfrak{D}'_{223} = \mathfrak{D}'_{232} = d_4$,

$$\mathfrak{D}' = \begin{bmatrix} \begin{pmatrix} 0 & 0 & d_4 \\ 0 & 0 & d_1 \\ d_3 & 0 & 0 \end{pmatrix} & \begin{pmatrix} 0 & 0 & -d_1 \\ 0 & 0 & d_4 \\ 0 & d_3 & 0 \end{pmatrix} & \begin{pmatrix} d_4 & -d_1 & 0 \\ d_1 & d_4 & 0 \\ 0 & 0 & d_2 \end{pmatrix} \end{bmatrix}. \tag{S62}$$

The equations of motion expressed using Euler angles simplify to

$$\begin{aligned} \dot{\phi} &= \tfrac{1}{2}(-2d_4 + d_3 + d_2 + (-2d_4 - d_3 + d_2)\cos 2\theta), \\ \dot{\theta} &= -d_1 \sin 2\theta, \\ \dot{\psi} &= 2d_4 \cos\theta. \end{aligned} \tag{S63}$$

Note that the dynamics of $\theta(t)$ is identical to that of the $D_{\infty h}$ particle: the C_{4h} particle aligns its 4-fold rotation axis parallel to the applied field when $d_1 > 0$ and perpendicular when $d_1 < 0$. It then continues to rotate steadily with a rate and direction that depends on its orientation. Particles aligned parallel to the field rotate at a rate d_2; those aligned perpendicular to the field rotate at a rate d_3. The stable fixed points are summarized as

$$\begin{aligned} &\theta = m\pi, \quad \dot{\phi} + (-1)^m \dot{\psi} = d_2 \quad \text{for} \quad d_1 > 0, \\ &\theta = (m + \tfrac{1}{2})\pi, \quad \dot{\phi} = d_3 \quad \text{fo} \quad d_1 < 0. \end{aligned} \tag{S64}$$

C_4 Particles: Spinning Rockets

The translation tensor in the particle frame $\mathfrak{C}'_{ijk}$ has four parameters: $\mathfrak{C}'_{333} = c_1$, $\mathfrak{C}'_{311} = \mathfrak{C}'_{322} = c_2$, $\mathfrak{C}'_{131} = \mathfrak{C}'_{113} = \mathfrak{C}'_{123} = \mathfrak{C}'_{132} = c_3$, and $-\mathfrak{C}'_{132} = -\mathfrak{C}'_{123} = \mathfrak{C}'_{113} = \mathfrak{C}'_{131} = c_4$,

$$\mathfrak{C}' = \begin{bmatrix} \begin{pmatrix} 0 & 0 & c_3 \\ 0 & 0 & c_4 \\ c_2 & 0 & 0 \end{pmatrix} & \begin{pmatrix} 0 & 0 & -c_4 \\ 0 & 0 & c_3 \\ 0 & c_2 & 0 \end{pmatrix} & \begin{pmatrix} c_3 & -c_4 & 0 \\ c_3 & c_4 & 0 \\ 0 & 0 & c_1 \end{pmatrix} \end{bmatrix}. \tag{S65}$$

As above, the particle is oriented such that its n-fold rotation axis is aligned parallel to the z'-axis. When the axis of the particle is oriented parallel to the applied field (Figure S11a), the particle moves parallel to its axis with speed c_1. When the axis is perpendicular to the field in its stable orientation (Figure S11b), the particle moves parallel to its axis with speed c_2. The other parameters c_3 and c_4 are needed only to describe transient particle motions during its rotation into the stable orientation.

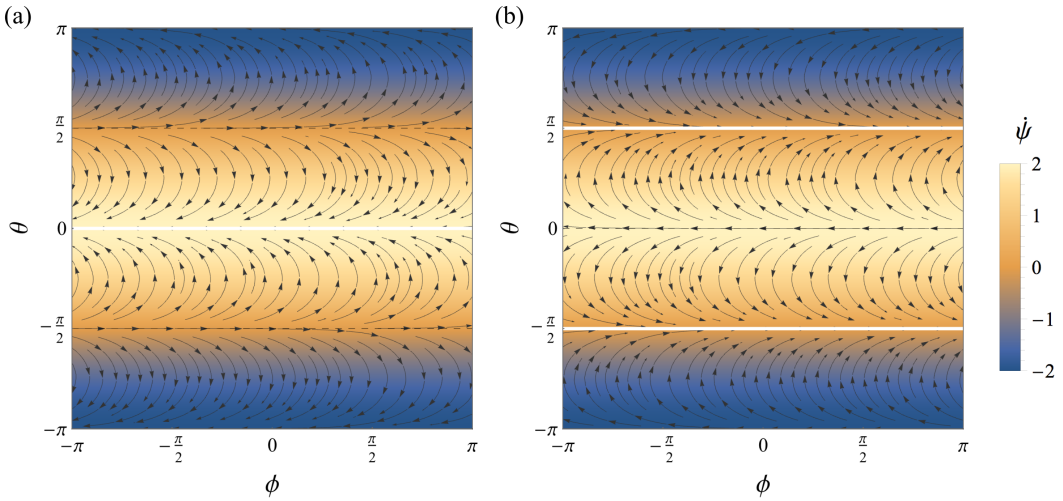

Figure S11: Phase portraits for the C_{4h} particle for (a) $d_1 = d_2 = d_3 = d_4 = 1$ and (b) $-d_1 = d_2 = d_3 = d_4 = 1$. The colormap shows the magnitude of $\dot{\psi}$; arrows show the flow in the $\phi\theta$ plane. Lines of stable fixed points are marked by white curves.

C_{3h} Particles: Spinning Gliders

The translation tensor in the particle frame $\mathfrak{C}'_{ijk}$ has two parameters: $-\mathfrak{C}'_{111} = \mathfrak{C}'_{122} = \mathfrak{C}'_{221} = \mathfrak{C}'_{212} = c_1$ and $-\mathfrak{C}'_{121} = -\mathfrak{C}'_{112} = -\mathfrak{C}'_{211} = \mathfrak{C}'_{222} = c_2$,

$$\mathfrak{C}' = \begin{bmatrix} \begin{pmatrix} -c_1 & -c_2 & 0 \\ -c_2 & c_1 & 0 \\ 0 & 0 & 0 \end{pmatrix} & \begin{pmatrix} -c_2 & c_1 & 0 \\ c_1 & c_2 & 0 \\ 0 & 0 & 0 \end{pmatrix} & \begin{pmatrix} 0 & 0 & 0 \\ 0 & 0 & 0 \\ 0 & 0 & 0 \end{pmatrix} \end{bmatrix}. \tag{S66}$$

As above, the particle is oriented such that its 3-fold rotation axis is aligned parallel to the z'-axis. When the axis of the particle is oriented parallel to the applied field (Figure S11a), the particle does not translate. When the axis is perpendicular to the field (Figure S11b), the particle moves perpendicular to its axis with speed $\sqrt{c_1^2 + c_2^2}$. Such gliding motions combined with spinning about the particle axis result in closed circular trajectories within planes parallel to the field.

S_4 Particles: Spinning Shuttles

The translation tensor in the particle frame $\mathfrak{C}'_{ijk}$ has four parameters: $-\mathfrak{C}'_{311} = \mathfrak{C}'_{322} = c_1$, $-\mathfrak{C}'_{131} = -\mathfrak{C}'_{113} = \mathfrak{C}'_{232} = \mathfrak{C}'_{223} = c_2$, $\mathfrak{C}'_{132} = \mathfrak{C}'_{123} = \mathfrak{C}'_{231} = \mathfrak{C}'_{213} = c_3$, and $\mathfrak{C}'_{312} = \mathfrak{C}'_{321} = c_4$,

$$\mathfrak{C}' = \begin{bmatrix} \begin{pmatrix} 0 & 0 & -c_2 \\ 0 & 0 & c_3 \\ -c_1 & c_4 & 0 \end{pmatrix} & \begin{pmatrix} 0 & 0 & c_3 \\ 0 & 0 & c_2 \\ c_4 & c_1 & 0 \end{pmatrix} & \begin{pmatrix} -c_2 & c_3 & 0 \\ c_3 & c_2 & 0 \\ 0 & 0 & 0 \end{pmatrix} \end{bmatrix}. \tag{S67}$$

As above, the particle is oriented such that its 2-fold rotation axis is aligned parallel to the z'-axis; the particle can be further rotated about that axis as to ensure that $c_4 = 0$. When the axis of the particle is oriented parallel to the applied field (Figure S11a), the particle does not translate. When the axis is perpendicular to the field (Figure S11b), the particle moves parallel with an orientation-dependent speed $c_1 \cos(2\phi)$. Such shuttling motions combined with spinning about the particle axis result in particle oscillations along a line perpendicular to the field.

4.5 S_6 Rotation Class

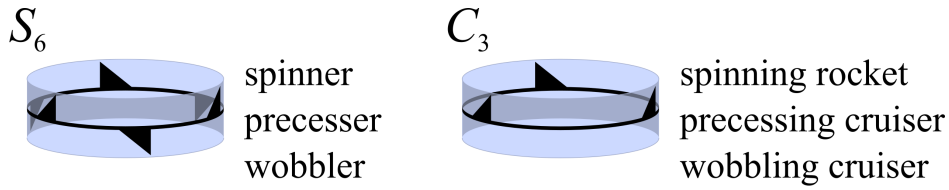

Figure S12: Schematic illustration of symmetry groups included in the S_6 rotation class. Particles with these symmetries exhibit the same rotational motions but differ in their translational motions.

Rotational Dynamics

The rotation tensor in the particle frame $\mathfrak{D}'_{ijk}$ can be expressed using five independent parameters: $-\mathfrak{D}'_{123} = -\mathfrak{D}'_{132} = \mathfrak{D}'_{213} = \mathfrak{D}'_{231} = d_1$, $\mathfrak{D}'_{333} = d_2$, $\mathfrak{D}'_{311} = \mathfrak{D}'_{322} = d_3$, $\mathfrak{D}'_{113} = \mathfrak{D}'_{131} = \mathfrak{D}'_{223} = \mathfrak{D}'_{232} = d_4$, and $-\mathfrak{D}'_{111} = \mathfrak{D}'_{122} = \mathfrak{D}'_{212} = \mathfrak{D}'_{221} = d_5$.

$$\mathfrak{D}' = \begin{bmatrix} \begin{pmatrix} -d_5 & 0 & d_4 \\ 0 & d_5 & d_1 \\ d_3 & 0 & 0 \end{pmatrix} & \begin{pmatrix} 0 & d_5 & -d_1 \\ d_5 & 0 & d_4 \\ 0 & d_3 & 0 \end{pmatrix} & \begin{pmatrix} d_4 & -d_1 & 0 \\ d_1 & d_4 & 0 \\ 0 & 0 & d_2 \end{pmatrix} \end{bmatrix}. \tag{S68}$$

Here, the particle is oriented such that its 3-fold rotation axis is aligned parallel to the z-axis; it is further rotated about that axis as to eliminate the components $\mathfrak{D}'_{121}$, $\mathfrak{D}'_{212}$, $\mathfrak{D}'_{211}$, and $\mathfrak{D}'_{222}$ from the rotation tensor. The equations of motion expressed using Euler angles simplify to

$$\begin{aligned} \dot{\phi} &= \tfrac{1}{2}\left[d_2 + d_3 - 2d_4 + (d_2 - d_3 - 2d_4)\cos 2\theta - d_5 \sin 2\theta \sin 3\phi\right], \\ \dot{\theta} &= d_5 \sin^2\theta \cos 3\phi - d_1 \sin 2\theta, \\ \dot{\psi} &= 2d_4 \cos\theta + d_5 \sin\theta \sin 3\phi. \end{aligned} \tag{S69}$$

Qualitatively, this particle can be viewed as a combination of a C_{4h} particle with a D_{3d} particle. When $d_1 > 0$, the particle aligns its rotation axis with the applied field an rotates steadily at a rate d_2 just like the C_{4h} particle. When $d_1 < 0$, the particle can adopt a either a fixed orientation or a complex rotational motion depending on the magnitude of d_5. When $d_5 = 0$, we recover the C_{4h} particle, which orients perpendicular to the field rotates steadily about its axis. For small d_5 (specifically, for $d_5^2 < 2[d_3(d_2 - 2d_4) + \sqrt{d_3^2(4d_1^2 + (d_2 - 2d_4)^2)}]$), the particle axis wobbles as it rotates. For sufficiently large d_5, the particle axis approaches a fixed orientation oblique to the field axis, about which the particle precesses at a steady rate.

C_3 Particles

The translation tensor in the particle frame $\mathfrak{C}'_{ijk}$ has six parameters: $-\mathfrak{C}'_{123} = -\mathfrak{C}'_{132} = \mathfrak{C}'_{213} = \mathfrak{C}'_{231} = c_1$, $\mathfrak{C}'_{333} = c_2$, $\mathfrak{C}'_{311} = \mathfrak{C}'_{322} = c_3$, $\mathfrak{C}'_{113} = \mathfrak{C}'_{131} = \mathfrak{C}'_{223} = \mathfrak{C}'_{232} = c_4$, and $-\mathfrak{C}'_{111} = \mathfrak{C}'_{122} = \mathfrak{C}'_{212} = \mathfrak{C}'_{221} = c_5$, and $\mathfrak{C}'_{112} = \mathfrak{C}'_{121} = \mathfrak{C}'_{211} = -\mathfrak{C}'_{222} = c_6$

$$\mathfrak{D}' = \begin{bmatrix} \begin{pmatrix} -c_5 & c_6 & c_4 \\ c_6 & c_5 & c_1 \\ c_3 & 0 & 0 \end{pmatrix} & \begin{pmatrix} c_6 & c_5 & -c_1 \\ c_5 & -c_6 & c_4 \\ 0 & c_3 & 0 \end{pmatrix} & \begin{pmatrix} c_4 & -c_1 & 0 \\ c_1 & c_4 & 0 \\ 0 & 0 & c_2 \end{pmatrix} \end{bmatrix}. \tag{S70}$$

As above, the particle is oriented such that its 3-fold rotation axis is aligned parallel to the z'-axis. When the axis of the particle is oriented parallel to the applied field (Figure S13a), the particle translates along its axis with velocity c_2. When the particle axis is wobbling (Figure S13b), it traces a complex trajectory that displaces the particle by a constant amount in any direction during each rotation cycle. When the particle axis is precessing (Figure S13c), it traces a helical trajectory parallel to the field.

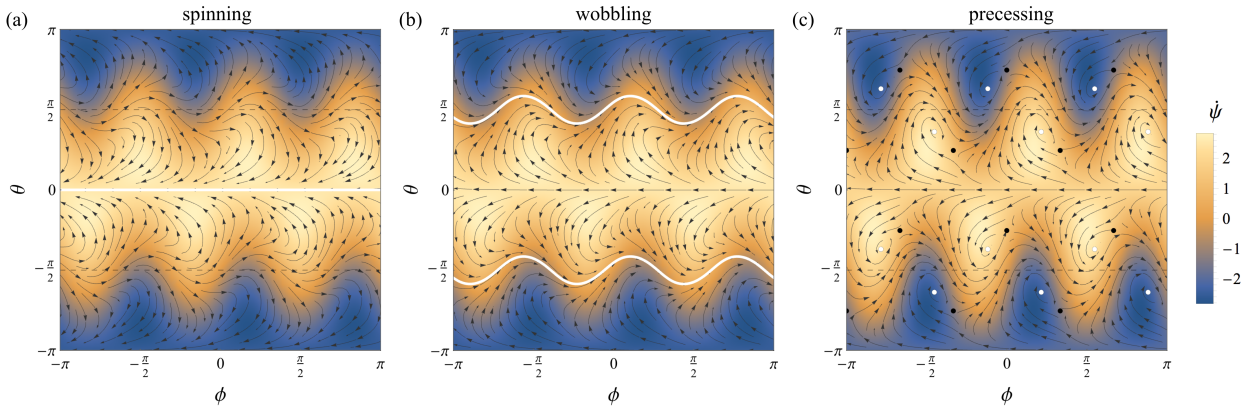

Figure S13: Phase portraits for the S_6 particle for (a) $d_1 = d_2 = d_3 = d_4 = d_5 = 1$, (b) $-d_1 = d_2 = d_3 = d_4 = d_5 = 1$, and (c) $-d_1 = d_2 = d_3 = d_4 = 1$ and $d_5 = 2$. The colormap shows the magnitude of $\dot{\psi}$; arrows show the flow in the $\phi\theta$ plane. Lines of stable fixed points are marked by white curves.

4.6 C_{2h} Rotation Class

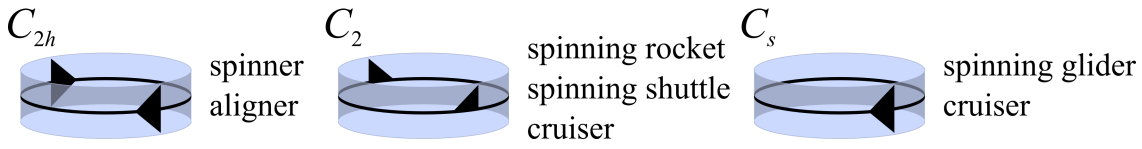

Figure S14: Schematic illustration of symmetry groups included in the C_{2h} rotation class. Particles with these symmetries exhibit the same rotational motions but differ in their translational motions.

Rotational Dynamics

The rotation tensor in the particle frame $\mathfrak{D}'_{ijk}$ can be expressed using eight parameters: $\mathfrak{D}'_{333} = d_1$, $\mathfrak{D}'_{322} = d_2$, $\mathfrak{D}'_{312} = \mathfrak{D}'_{321} = d_3$, $\mathfrak{D}'_{311} = d_4$, $\mathfrak{D}'_{232} = \mathfrak{D}'_{223} = d_5$, $\mathfrak{D}'_{231} = \mathfrak{D}'_{213} = d_6$, $\mathfrak{D}'_{132} = \mathfrak{D}'_{123} = d_7$, and $\mathfrak{D}'_{131} = \mathfrak{D}'_{113} = d_8$,

$$\mathfrak{D}' = \begin{bmatrix} \begin{pmatrix} 0 & 0 & d_8 \\ 0 & 0 & d_6 \\ d_4 & d_3 & 0 \end{pmatrix} & \begin{pmatrix} 0 & 0 & d_7 \\ 0 & 0 & d_5 \\ d_3 & d_2 & 0 \end{pmatrix} & \begin{pmatrix} d_8 & d_7 & 0 \\ d_6 & d_5 & 0 \\ 0 & 0 & d_1 \end{pmatrix} \end{bmatrix}. \tag{S71}$$

Here, the particle is oriented such that its 2-fold rotation axis is aligned parallel to the z-axis. Note that the particle can be rotated about its axis to eliminate one the above parameters (e.g., such that $d_3 \to 0$). The equations of motion expressed using Euler angles simplify to

$$\begin{aligned} \dot{\phi} &= [A + B\cos 2\phi - C\sin 2\phi]\cos^2\theta + \tfrac{1}{2}[D + E\cos 2\phi]\sin^2\theta, \\ \dot{\theta} &= \tfrac{1}{2}[F + C\cos 2\phi + B\sin 2\phi]\sin 2\theta, \\ \dot{\psi} &= [G - B\cos 2\phi + C\sin 2\phi]\cos\theta, \end{aligned} \tag{S72}$$

where $A = d_1 - d_5 - d_8$, $B = d_8 - d_5$, $C = d_6 + d_7$, $D = d_2 + d_4$, $E = d_2 - d_4$, $F = d_7 - d_6$, and $G = d_5 + d_8$. Qualitatively, this particle can be viewed as a combination of a C_{4h} particle with a D_{2h} particle. For the conditions below, the particle aligns its rotation axis with the applied field ($\theta = 0$) an rotates steadily at a constant rate just like the C_{4h} particle (Figure S15 a,b),

$$\left(A^2 > B^2 + C^2 \text{ and } F < 0\right) \text{ or } \left(A^2 < B^2 + C^2 \text{ and } F < -\sqrt{B^2 + C^2 - A^2}\right). \tag{S73}$$

For other conditions, the particle aligns its rotation axis perpendicular to the applied field ($\theta = \pi/2$) and rotates about that axis at a variable rate (Figure S15c). This behavior is stable provided that

$$E^2 > F^2 \text{ and } F > 0. \tag{S74}$$

If neither condition (S73) nor (S74) is satisfied, then the particle adopts a stable orientation with its axis oblique to that of the field (Figure S15d).

C_2 Particles

The translation tensor in the particle frame $\mathfrak{C}'_{ijk}$ has eight parameters: $\mathfrak{C}'_{333} = c_1$, $\mathfrak{C}'_{322} = c_2$, $\mathfrak{C}'_{312} = \mathfrak{C}'_{321} = c_3$, $\mathfrak{C}'_{311} = c_4$, $\mathfrak{C}'_{232} = \mathfrak{C}'_{223} = c_5$, $\mathfrak{C}'_{231} = \mathfrak{C}'_{213} = c_6$, $\mathfrak{C}'_{132} = \mathfrak{C}'_{123} = c_7$, and $\mathfrak{C}'_{131} = \mathfrak{C}'_{113} = c_8$,

$$\mathfrak{C}' = \begin{bmatrix} \begin{pmatrix} 0 & 0 & c_8 \\ 0 & 0 & c_6 \\ c_4 & c_3 & 0 \end{pmatrix} & \begin{pmatrix} 0 & 0 & c_7 \\ 0 & 0 & c_5 \\ c_3 & c_2 & 0 \end{pmatrix} & \begin{pmatrix} c_8 & c_7 & 0 \\ c_6 & c_5 & 0 \\ 0 & 0 & c_1 \end{pmatrix} \end{bmatrix}. \tag{S75}$$

As above, the particle is oriented such that its 3-fold rotation axis is aligned parallel to the z'-axis. When the axis of the particle is oriented parallel to the applied field (Figure S15a,b), the particle translates along

its axis with velocity c_1. When the axis of the particle is oriented perpendicular to the applied field (Figure S15c), the particle translates along its axis with a steady velocity $\frac{1}{2}(c_2+c_4)$ superimposed with an oscillatory component of magnitude $[c_3^2 + \frac{1}{4}(c_4 - c_2)^2]^{1/2}$. This behavior combines the steady translation of a rocket with the oscillatory translation of a shuttle. Finally, when the particle adopts a fixed orientation in the field (Figure S15d), it can translate along any direction at a constant rate (as determined by its shape and orientation about the field axis).

C_s Particles

The translation tensor in the particle frame $\mathfrak{C}'_{ijk}$ has ten parameters: $\mathfrak{C}'_{332} = \mathfrak{C}'_{323} = c_1$, $\mathfrak{C}'_{331} = \mathfrak{C}'_{313} = c_2$, $\mathfrak{C}'_{233} = c_3$, $\mathfrak{C}'_{222} = c_4$, $\mathfrak{C}'_{221} = \mathfrak{C}'_{212} = c_5$, $\mathfrak{C}'_{211} = c_6$, $\mathfrak{C}'_{133} = c_7$, $\mathfrak{C}'_{122} = c_8$, $\mathfrak{C}'_{121} = \mathfrak{C}'_{112} = c_9$, and $\mathfrak{C}'_{111} = c_{10}$,

$$\mathfrak{C}' = \begin{bmatrix} \begin{pmatrix} c_{10} & c_9 & 0 \\ c_6 & c_5 & 0 \\ 0 & 0 & c_2 \end{pmatrix} & \begin{pmatrix} c_9 & c_8 & 0 \\ c_5 & c_4 & 0 \\ 0 & 0 & c_1 \end{pmatrix} & \begin{pmatrix} 0 & 0 & c_7 \\ 0 & 0 & c_3 \\ c_2 & c_1 & 0 \end{pmatrix} \end{bmatrix}. \tag{S76}$$

Here, the particle is oriented such that its plane of mirror symmetry is perpendicular to the z'-axis. When the z'-axis of the particle is oriented parallel to the applied field (Figure S15a,b), the particle translates along with speed $(c_3^2 + c_7^2)^{1/2}$ along a circular trajectory within the plane perpendicular to the field. When the z'-axis of the particle is oriented perpendicular to the applied field (Figure S15c), the particle translates perpendicular to that axis with a speed and direction that depends on its orientation ϕ about the axis. Combined with rotation at an orientation-dependent rate, the particle executes complex periodic orbits within a plane parallel to the field. Finally, when the particle adopts a fixed orientation in the field (Figure S15d), it can translate along any direction at a constant rate (as determined by its shape and orientation about the field axis).

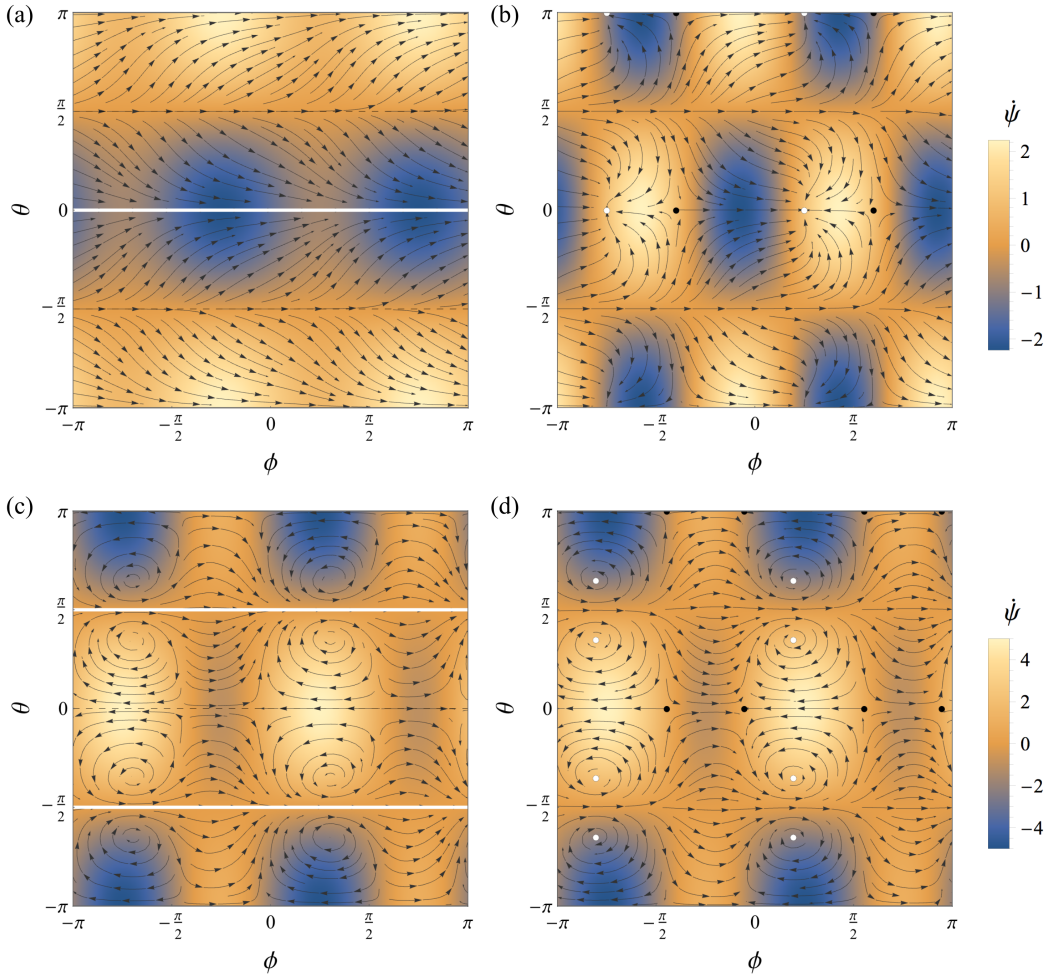

Figure S15: Phase portraits for the C_{2h} particle for $d_3 = 0$ and (a) $d_1 = d_2 = d_4 = -d_5 = \frac{1}{2}d_6 = -d_7 = -d_8 = 1$, (b) $d_1 = d_2 = d_4 = -d_5 = \frac{1}{2}d_6 = -d_7 = d_8 = 1$, (c) $d_1 = d_2 = d_4 = d_5 = d_6 = \frac{1}{2}d_7 = d_8 = 1$, and (d) $d_1 = d_2 = d_4 = d_5 = \frac{1}{2}d_6 = d_7 = d_8 = 1$. The colormap shows the magnitude of $\dot{\psi}$; arrows show the flow in the $\phi\theta$ plane. Stable fixed points are marked by white dots; lines of stable fixed points are denoted by white curves. Note that the stable dynamics for (a) and (b) are physically identical: the particle orients parallel to the field ($\theta = 0$) at rotates at a steady velocity $\dot{\phi} + \dot{\psi} = d_1$.

5 Sensitivity on Particle Shape

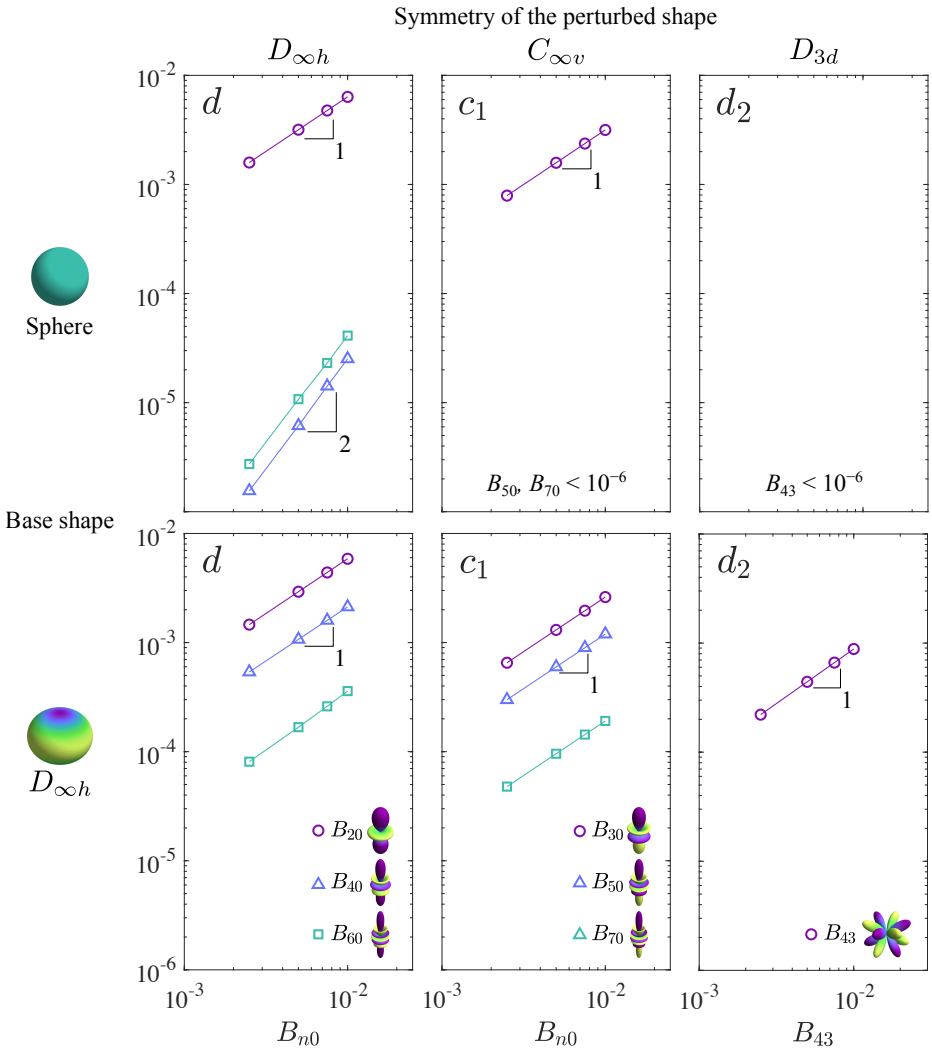

Figure S16: Changes in selected components of the shape tensors as a function of three different shape perturbations (columns): addition of spherical harmonics Y_n^0 for even n ($D_{\infty h}$ symmetry), Y_n^0 for odd n ($C_{\infty v}$ symmetry), and Y_4^3 (D_{3d} symmetry). The effects of these perturbations depend qualitatively on the unperturbed "base shape" – here, a sphere (top row) and a perpendicular aligner with $B_{20} = -0.2$ (bottom row). The plots show the responses for the orientation parameter d for $D_{\infty h}$ particles (section 4.1), the translation parameter c_1 for $C_{\infty v}$ particles (section 4.1), and the rotation parameter d_2 for D_{3d} particles (section 4.3).

6 Effects of Brownian Motion

$D_{\infty h}$ Particles

We consider the dynamics of a parallel aligner with $D_{\infty h}$ symmetry (Fig. 2a). In the absence of Brownian motion, such particles align their primary axis parallel to the field. We simulated the dynamics of a particular $D_{\infty h}$ particle in the presence of Brownian motion for different dimensionless temperatures $\beta = k_B T/a^3 \varepsilon E_\infty^2$. The plot below shows the particle orientation θ_x and the rotational mean-square-displacement (MSD) as a function of time (Fig. S17). The angle θ_x is defined by projecting the particle's z' axis (vector $[0, 0, 1]$ in the particle frame) onto the yz plane in the lab frame. The angle $\theta_x(t)$ is defined as the angle of rotation around the x axis between this projected vector at time t and the same vector at time zero. We count each full counterclockwise rotation as an addition of 2π, and similarly we subtract 2π for each full clockwise rotation. The rotational MSD is then defined as

$$\mathrm{MSD}(t) = \left\langle \left(\theta_x(t'+t) - \theta_x(t')\right)^2 \right\rangle. \tag{S77}$$

At low temperatures (e.g., $\beta = 0.3$), the particle orientation fluctuates about one stable orientation but does not "flip" to the other orientation on the time scale of the simulations. At higher temperatures (e.g., $\beta = 1.2$), the particle flips stochastically giving rise to diffusive behavior at long times – that is, $\mathrm{MSD}(t) \propto t$.

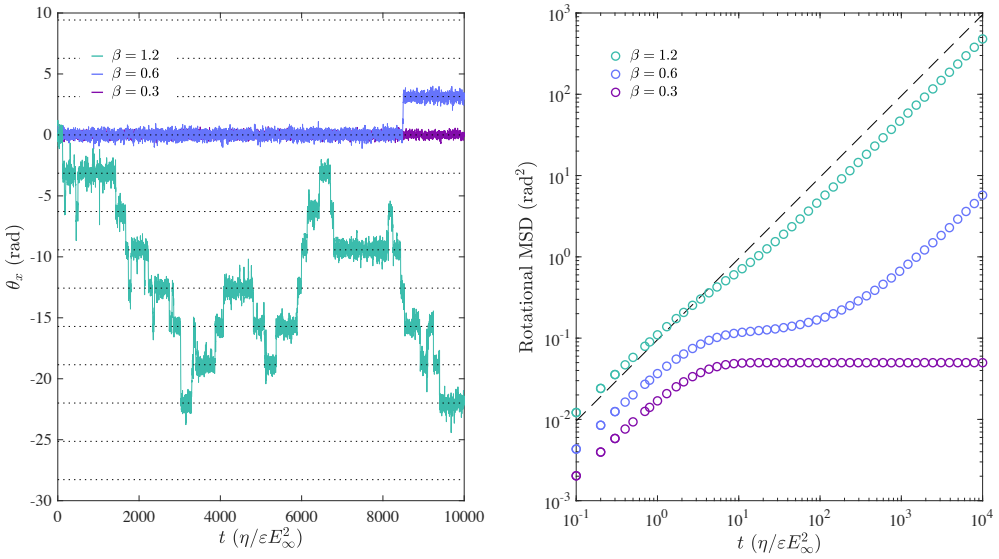

Figure S17: Parallel aligner with $D_{\infty h}$ symmetry. (left) Particle orientation θ_x as a function of time for three different temperatures $\beta = k_B T/a^3 \varepsilon E_\infty^2$. Particle shape is characterized by $B_{20} = 0.4$. (right) Rotational mean-squared-displacement as a function of time for the same three temperatures. The dashed curve is $2D_r t$ with diffusivity $D_r = k_B T/8\pi\eta a^3$ like that of a spherical particle ($\beta = 1.2$).

$C_{\infty v}$ Particles

Rockets with $C_{\infty v}$ symmetry are in the same rotation class as the aligner ($D_{\infty h}$) and therefore exhibit the same rotational motions. Additionally, rockets can translate parallel to their axis at a constant rate (Fig. 3c and d). We simulated the dynamics of such particles in the presence of Brownian motion for different dimensionless temperatures $\beta = k_B T/a^3 \varepsilon E_\infty^2$ and computed the translational MSD in the x, y, and z directions (Fig. S18). Owing to the symmetry of the applied field, the MSD in the x and y directions were equal and therefore averaged together. At low temperatures, the MSD of the parallel rocket in the z-direction increased quadratically in time corresponding to steady ICEP translation. At higher temperatures, particle motions in all directions became diffusive at long times due to diffusion-induced transitions between the

particle's different stable orientations. The effective diffusivity in the z direction is significantly greater than that in the xy directions. In this regime, ICEP motions result in enhanced and anisotropic particle diffusion. Similar behaviors are observed at higher temperatures; however, the magnitude of diffusion enhancement and anisotropy are diminished.

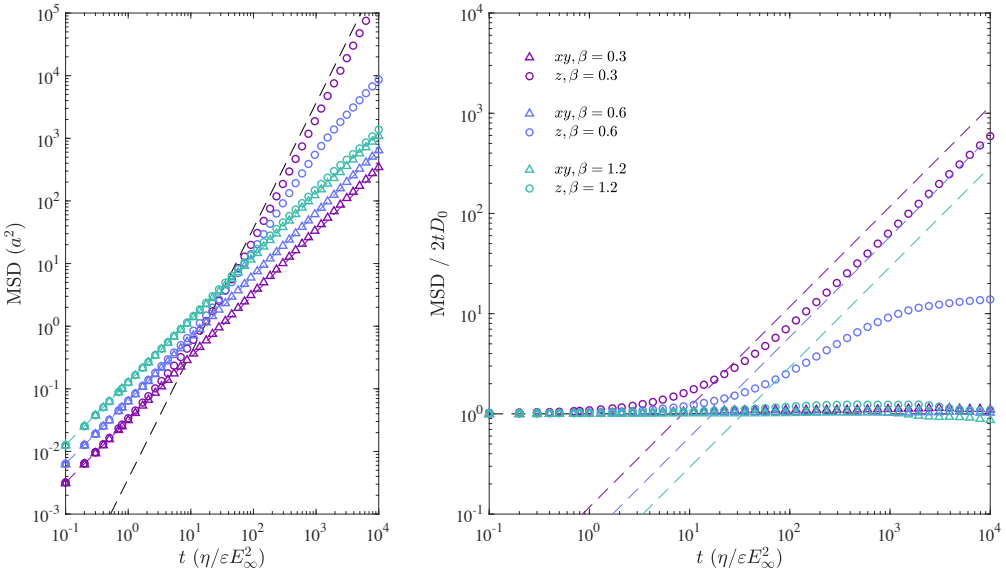

Figure S18: Parallel rockets with $C_{\infty v}$ symmetry. (left) Translational mean-squared-displacement (MSD) of a $C_{\infty v}$ parallel rocket as a function of time for three different temperatures $\beta = k_B T/a^3 \varepsilon E_\infty^2$. The dashed curves show the expectation based on diffusion alone $2tD_0$ with isotropic diffusivity $D_0 = k_B T |\boldsymbol{R}_{FU}|^{-1/3}$. Particle shape is characterized by $B_{30} = B_{20} = 0.2$. (right) Calculated MSD scaled by $2tD_0$ function of time for the same three temperatures. The dashed curves show the expectation for steady translation in the z-direction in the absence of Brownian motion.

D_3 Particles

The deterministic dynamics of a perpendicular flipping glider with D_3 symmetry is similar to that of the parallel rocket above; however, it stochastic dynamics is quite different (Fig. S19). In particular, the D_3 particle shows significant enchancements in the diffusivity in the directions perpendicular to the field. Such enhancements may be due to the hydrodynamic coupling of rotation and translation characteristic of particles of D_3 symmetry.

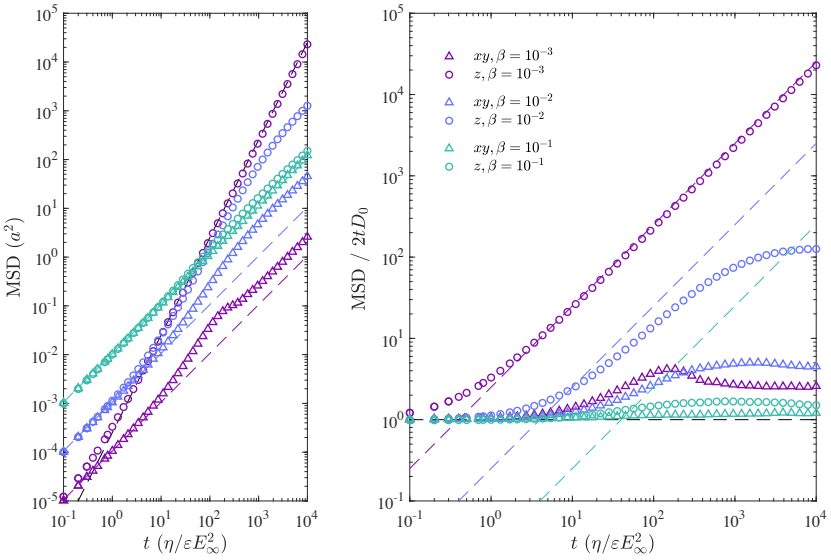

Figure S19: Perpendicular flipping glider with D_3 symmetry. (left) Translational mean-squared-displacement (MSD) as a function of time for three different temperatures $\beta = k_BT/a^3\varepsilon E_\infty^2$. The dashed curves show the expectation based on diffusion alone $2tD_0$ with isotropic diffusivity $D_0 = k_BT|\boldsymbol{R}_{FU}|^{-1/3}$. Particle shape is characterized by $iB_{43} = iB_{33} = -B_{30} = B_{20} = -0.2$. (right) Calculated MSD scaled by $2tD_0$ function of time for the same three temperatures. The dashed curves show the expectation for steady translation in the z-direction in the absence of Brownian motion.

7 Two-Photon Lithography

To demonstrate the ability to fabricate colloidal particles with prescribed shapes, we used two-photon lithography to create a physical realization of a C_2 particle with radius of 5 microns (Fig. S20c). We used Mathematica to generate a three-dimensional model of a particle specified by the spherical harmonic coefficients $B_{30} = 0.6$, $B_{22} = 0.8$, and $B_{44} = 0.5i$. This model was then printed on a glass coverslip using a Nanoscribe Photonic Professional GT available through the nanofabrication facilities at the Materials Research Institute at the Pennsylvania State University. Electron microscopy images were taken using a Zeiss SIGMA VP-FESEM available at the Huck Institutes of the Life Sciences at the Pennsylvania State University.

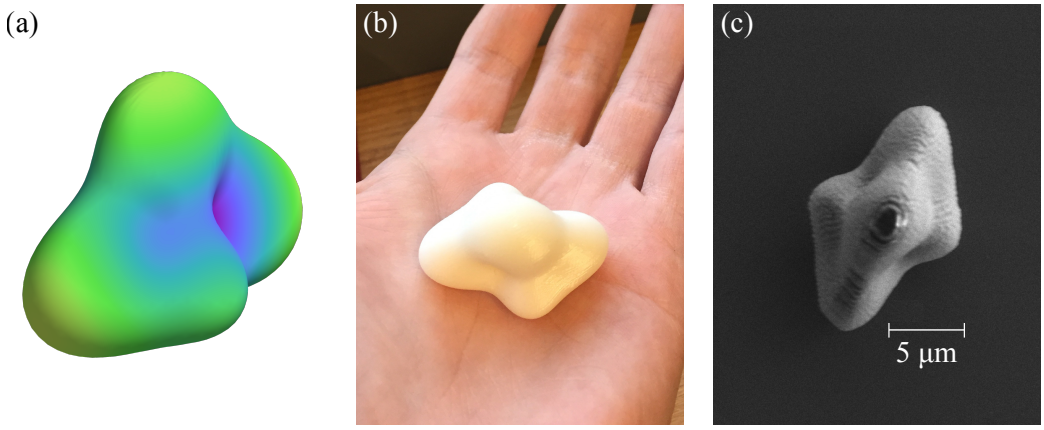

Figure S20: (a) A particle with C_2 symmetry specified by basis function weights $B_{30} = 0.6$, $B_{22} = 0.8$, and $B_{44} = 0.5i$. (b) The same C_2 particle printed at the macro-scale using a conventional 3D printer. (c) SEM image of the same C_2 particle printed at the micro-scale using a Nanoscribe Photonic Professional GT two-photon lithography tool.

References

(1) Cotton, F. A., *Chemical Applications of Group Theory*, 3rd; Wiley-Interscience: 1990.

(2) Pozrikidis, C., *A Practical Guide to Boundary Element Methods with the Software Library BEMLIB*; CRC Press: 2002.

(3) Stone, H.; Samuel, A. *Phys. Rev. Lett.* **1996**, *77*, 4102–4104.

(4) Squires, T. M.; Bazant, M. Z. *J. Fluid Mech.* **2006**, *560*, 65–101.

(5) Lebedev, V. I. *USSR Comput. Math. Math. Phys.* **1976**, *16*, 10–24.

(6) Swan, J. W.; Brady, J. F. *J. Fluid Mech.* **2011**, *687*, 254–299.